Catchment-scale conceptual modelling of water and solute transport in the dual flow system of the karst critical zone

Zhicai Zhang[1,2,3], Xi Chen[2,3]*, Chris Soulsby[1]

1: School of Geosciences, University of Aberdeen, Aberdeen AB24 3UF, United Kingdom
2: State Key Laboratory of Hydrology-Water Resources and Hydraulic Engineering Hohai University, Nanjing 210098, China
3: College of hydrology and water resources, Hohai University, Nanjing 210098, China

*Corresponding author
E-mail: zhangzhicai_0@hhu.edu.cn (Z.C. Zhang), xichen@hhu.edu.cn (X. Chen), c.soulsby@abdn.ac.uk (C. Soulsby)

Submitted to Hydrological Processes

Key points

1 We developed a conceptual model that combines a dual reservoir runoff model combined with ARMA model for the karst critical zone;

2 We estimated bidirectional flow and solute exchange between fracture and conduit networks in three nested catchments with different karst critical zone architectures;

3 Sinkholes have significant influence on contribution of various flows to catchment outlet and mass export.

This article has been accepted for publication and undergone full peer review but has not been through the copyediting, typesetting, pagination and proofreading process which may lead to differences between this version and the Version of Record. Please cite this article as doi: 10.1002/hyp.11268

Abstract

Hydrological and hydrochemical processes in the critical zone of karst environments are controlled by the fracture-conduit network. Modelling hydrological and hydrochemical dynamics in such heterogeneous hydrogeological settings remains a research challenge. In this study, water and solute transport in the dual flow system of the karst critical zone were investigated in a 73.5km^2 catchment in southwest China. We developed a dual reservoir conceptual runoff model combined with an ARMA model with algorithms to assess dissolution rates in the "fast flow" and "slow flow" systems. This model was applied to three catchments with typical karst critical zone architectures, to show how flow exchange between fracture and conduit networks changes in relation to catchment storage dynamics. The flux of bidirectional water and solute exchange between the fissure and conduit system increase from the headwaters to the outfall due to the large area of the developed conduits and low hydraulic gradient in the lower catchment. Rainfall amounts have a significant influence on partitioning the relative proportions of flow and solutes derived from different sources reaching the underground outlet. The effect of rainfall on catchment function is modulated by the structure of the karst critical zone (e.g. epikarst and sinkholes). Thin epikarst and well-developed sinkholes in the headwaters divert more surface water (younger water) into the underground channel network, leading to a higher fraction of rainfall recharge into the fast flow system and total outflow. Also, the contribution of carbonate weathering to mass export is also higher in the headwaters due to the infiltration of younger water with low solute concentrations through sinkholes.

Key words: karst critical zone; dual flow system; conceptual model; flow and solute; bidirectional exchange

1 Introduction

Flow systems in karst areas are complex due to the unique geomorphology and structure of carbonate rocks. Unlike non-karst areas where water is stored and flows in a relatively uniform matrix of soil and bedrock, karst water is characteristically stored and flows in complex subterranean drainage networks of fracture and conduit systems that usually discharge at large springs (Bonacci, 1987). At the same time, conduit flow interacts with its surrounding matrix and exchanges frequently with water in the small fractures or soil depending on the prevailing hydraulic gradient (Bailly-Comte et al, 2010). This mixed-flow system integrates components with various flow velocities, e.g. low velocities in the fissures and fracture volumes and high flow velocities in the conduit/channel network (Field, 1993; Quinlan and Ewers, 1985), with associated transitions between states of laminar and turbulent flow (White, 2007; Worthington, 2009).

Water flowing through carbonate rocks is enriched with chemical solutes and can potentially take up a significant amount of inorganic carbon (White, 1988; Katz et al., 1997; Liu et al., 2010a). The chemical composition of natural waters comes from the dissolution of minerals and gases, and the alteration of previously dissolved components due to precipitation and other processes. In karst areas, due to the high influence of flow variability on carbonate dissolution, the concentrations of inorganic geochemicals in groundwater exhibits strong temporal and spatial variation (Li et al, 2008). A major controlling factor is mixing during hydrological events; this usually causes a sharp change in solute concentration, which strongly correlates with discharge fluctuation.

Simulation of hydrological processes in karst systems has been mostly achieved using

two main modelling methods: physically distributed models and lumped models. Distributed modelling of groundwater dynamics, such as MODFLOW-DCM (Sun et al., 2005), can be adapted to represent the flow conditions in dual porosity systems comprising an underground conduit-and-fracture network embedded within a porous matrix for integrated simulation of flow and solute transport in karst environments (Birk et al, 2006; Ronayne 2013). Such distributed models need detailed knowledge about the spatial distribution of the fracture network and a large number of parameters, such as hydraulic conductivities and storage coefficients for different units in complex karst aquifers. For this reason, simpler lumped models are often preferred (Ghasemizadeh et al, 2012; Ladouche et al, 2014; Arfib and Charlier, 2016). As the temporal variations of spring discharge, usually observed at conduit outflows, reflects the overall hydrogeological configuration of karst aquifers. Time series analyses are commonly applied to transform input signals (recharge) into output signals (discharge) and can identifying systematic and cyclic variations, e.g. time-lags or memory effect. However, these analyses cannot provide direct information concerning aquifer hydraulic processes (Kovacs, 2003). These can be captured by conceptual models or lumped parameter models which are based on simpler representation of physical phenomena. Consequently, they can provide significant insight into the overall functioning of a karst system. A popular way to convert a conceptual model of a groundwater system into mathematical formulations are reservoir (or 'tank') type models (Sugawara, 1995; Rimmer and Hartmann, 2012; Chang et al, 2017), which can represent dual flow (fast and slow flow) systems for simulation of water and solute fluxes (Pinault et al, 2001; Charlier et al, 2012;

Hartmann et al, 2013). Nevertheless, observations are usually made of only one element of the flow system, most commonly discharge at the conduit/channel at the catchment outlet as a basis for model calibration. Therefore, combining conceptual models with time series analyses for water and solute transport can help identify appropriate model structures, using behavioural traits such as memory effects to determine the number of reservoir units and their interlinkages, and associated model parameters. These can be tested against observed data of spring discharge and hydrochemical tracers (Hartmann et al, 2013).

One of the largest, continuous karst areas in the world is located in Yunnan-Guizhou Plateau of southwest China, which also has a population of 100 million. Carbonate rocks occupy 41.31% of the total area of 730.6×10^3 km^2. The highly transmissive karst structure means that rainfall is quickly routed through the often thin soils. Groundwater is a primary water resource supporting social and economic development and ecosystem recovery under karst desertification. Thus, it is crucial to understand the hydrology of the karst critical zone to provide an evidence base for sustainable land and water management. Owing to the different solution kinetics of Mg and Ca minerals, the use of solute concentrations from soluble carbonate rock as tracers has the potential to help understand the geochemical evolution and mixing of water from different sources, (e.g. groundwater flow paths and hydraulic connections) within a complex karst drainage network.

A focus for critical zone research within the South West China karst region is the $73.5km^2$ Houzhai catchment in Guizhou province. This catchment has typical karst critical zone architectures, which change moving from the upland headwaters to the lowlands. Previous

work has characterised the hydrology and hydrochemistry of this catchment or sub-catchments (Liu, et al, 2010a; Zhao et al, 2010; Yan et al, 2012; Zhang et al, 2013) and hydrological models of the dual flow system have been developed (Liu et al, 2010b; Zhang, et al, 2011; Chen et al, 2013). Here we seek to advance these models integrating important hydrochemical processes in a conceptual flow model to simulate both the discharge and solute output from the catchment. Use of hydrochemical tracers in such models can help test whether they give "the right answers for the right reasons" (Kirchner, 2006). The specific aims of the paper are: (1) to develop a conceptual hydrochemical model that links the reservoir type model with time series analysis and couples simulation of the dual flow system (fracture and conduit/channel) with evolution of solutes mobilized by the dissolution of carbonate rock; (2) to calibrate and test the coupled model using available observation data of streamflow discharge and solute concentration at three different scales; (3) to quantify contributions of different water sources to the streamflow and chemical export at contrasting scales and assess how these change with catchment characteristics.

2 Study catchment and Data

2.1 Catchment characteristics

The Houzhai catchment has an area of 73.5 km^2 and is located in Puding County, Guizhou Province in southwest China. (Figure 1(a)). The catchment has a subtropical wet monsoon climate. The mean annual temperature is 20.1^oC, highest in July and lowest in January. Annual precipitation is 1300 mm, with a distinct summer wet season and a winter dry season and the annual potential evaporation is approximately 920 mm. The topography of

the study catchment is high and steep in the eastern mountainous area and low and gentle in the western plain. The elevation ranges from 1218 to 1565 m above sea level. In the east, many peak-cluster depressions are surrounded by karst mountainous peaks, forming the typical cone and cockpit karstic geomorphology of southwest China. The soils are thin (less than 50cm). The steep hillslopes in the east are covered with very thin, discontinuous limestone soil and the plain area in the west is covered with paddy soil. Forest is cover is highest in the uncultivated steeper mountains and agriculture is dominant in the cultivated depressions.

The aquifer system in the study area consists of mainly limestone and dolomite of the Middle Triassic Guanling Formation (Figure 1(b)). From the oldest to the youngest of the lithology, the geology can be divided into interbedded shale and marlstone (T^2g^1), limestone with vermicular limestone (T^2g^{2-1}) , limestone with marlstone (T^2g^{2-2}), limestone (T^2g^{2-3}) and dolomite (T^2g^3) (Yang, 2001), with different composition of the carbonate rocks and thus dissolution capacity. It was estimated that the ratio of CaO/MgO is 48, 28, 30 and 3 for T^2g^{2-1}, T^2g^{2-2}, T^2g^{2-3} and T^2g^3, respectively (Yu et al., 1990). Spatial difference of the carbonate rock properties and discharge leads to marked heterogeneity of fractures and conduits/conduits in space. Apertures of fractures and fissures range from less than 1mm to larger than 5mm in the karst profile with the hydraulic conductivity ranging of 10^{-3}~10^{-7} m/s (Freeze and Cherry, 1979), and conduits/channels in the ranges of several centimeters to several meters.

The underground channel in the south of the catchment originates from the eastern

mountainous area where most surface and subsurface flow recharges into the underground channel through the sinkholes. It stretches to a relatively flat plain in the middle and lower catchment (Figure 1(a)). The underground channel is well-developed and connects numerous larger fractures. The depth of the deep flow zone (i.e. the underground channel bed or lower watershed boundary) is about 20-40m below the ground surface (Yu et al., 1990). Within the Houzhai catchment, there are three permanent gauging stations at Muzhudong (MZD), Laoheitan (LHT) and Maoshuikeng (MSK) located in the upper, middle and downstream (outlet) parts of the underground channel (Figure 1(a)), respectively. The estimated areas are 6.1, 18.5 and 73.5 km^2 for MZD, LHT and MSK, respectively, according to geomorphologic conditions and the underground channel network.

This catchment is rich in sinkholes in depression areas (Figure 1(c)). Sinkholes receive concentrated recharge of lateral surface and subsurface flows in the epikarst zone and directly drain into the underground channels, resulting in a sharp rise and drop of the hydrograph. Based on the data of DEM and field survey, the drainage area of sinkholes after heavy rain was identified by using ARCGIS. The total drainage area for these sub-catchments at MZD, LHT and MSK is 4.51, 9.43 and 15.5 km^2, respectively.

2.2 Hydro-chemical observation data

Flow discharge and precipitation were measured daily at the three gauging stations over a five-year period from 1 January 1997 to 31 December 2001 (apart from a missing year in 2000 at MSK). The concentration of a suite of chemical ions (e.g. Ca, Mg, K, Na, HCO_3, SO_4, Cl) were analysed in the laboratory from water samples collected at weekly intervals in

the wet season from May to October, and fortnightly in the dry season. Since concentrations of most weathering-derived elements were strongly co-correlated, the dissolution of carbonate rocks in groundwater could be indexed by the sum of Mg^{2+} and Ca^{2+}. The total of concentration of Mg^{2+} and Ca^{2+}, sometimes used to define water hardness, were used as index of dissolved carbonate rock in this study. The concentration of Mg^{2+} and Ca^{2+} in rain water is much lower than that in catchment waters (Yu, 1990). In this study, the mean value of 4.5 mg/L from preliminary results by Yu (1990) was used to represent the total concentration of Mg^{2+} and Ca^{2+} in rain water.

3 Methodology

Due to the strong heterogeneity of the karst fracture system, flow in the larger conduits is much faster than that in the surrounding carbonate rocks (fracture-matrix) (Zhang et al, 2013). The behaviour of karst spring hydrographs can, in principle, be simulated using a two-reservoir model that conceptualises the dual flow system (Figure 2). The low permeability “slow flow” reservoir represents the fractured matrix blocks of the aquifer and the highly permeable “fast flow” reservoir represents the larger karst conduits. In terms of mass balance and exchange of fluxes between the two reservoirs, mathematical equations to calculate the underground flow and solute concentration in the dual flow system are developed as follows (with additional information in Appendix A).

3.1 Module of dual flow system

According to the process-based karst model introduced by Hartmann et al. (2013) , the equation used to describe water exchange between the two reservoirs depends on their difference in water tables is as follow:

$$Q_E = K_E A_{fc} \frac{h_2 - h_1}{\Delta x_{fc}} \quad (1)$$

where K_E is hydraulic conductivity between the two reservoirs (m/d), h_1, h_2 are the water table of fracture and conduit (m), respectively, A_{fc} is the equivalent cross-section of the connection (m^2), and Δx_{fc} is an average flow distance (m). Q_E can be calculated by:

$$Q_{E,t} = -\frac{V_{f,t} - fV_{s,t}}{k_e} \quad (2)$$

where $V_{s,t}$ and $V_{f,t}$ are water storage at time t in slow and fast flow reservoirs, respectively; $V_{f,t} = Ah_1 n_1$, and $V_{s,t} = Ah_2 n_2$; $f = \frac{n_1}{n_2}$, n_1 and n_2 are the porosity of the conduits and fracture matrix, respectively; k_e is coefficient of the equation associated with the catchment area A, f, n_2, Δx_{fc}, K_E and A_{fc} ($k_e = \frac{Afn_2 \Delta x_{fc}}{K_E A_{fc}}$).

The water balance equations in the slow and fast flow reservoirs at the time t can be expressed as:

for the slow reservoir: $\frac{dV_{s,t}}{dt} = I_{s,t} + \frac{V_{f,t} - fV_{s,t}}{k_e}$ (3)

for the fast reservoir: $\frac{dV_{f,t}}{dt} = I_{f,t} - \frac{V_{f,t} - fV_{s,t}}{k_e} - Q_{f,t}$ (4)

where $I_{s,t}$ and $I_{f,t}$ are rainfall recharge into the slow and fast flow reservoirs, respectively, from the upper epikarst zone, which can be calculated by $I_s = \alpha P * A_s/\Delta t$ and $I_f = \beta P * A_f/\Delta t$ (α and β are coefficients of precipitation recharge into the slow and fast flow reservoirs, respectively. A_s and A_f are the recharge areas of the slow and fast flow reservoirs, respectively).

Eqs (3) and (4) describe that precipitation falling in the upper epikarst directly recharges into the slow reservoir (diffuse recharge, I_s in Eq (3)) through the fracture area (A_s), and the fast reservoir or underground channel (preferential recharge, I_f in Eq (4)) through the vertically interconnected larger fracture and conduit (A_f). Typical epikarst profile investigations shows that vertically interconnected large fractures and conduits (preferential recharge area A_f) occupy about 8% of the epikarst zone (Zhang et al.,2013) and the remaining small fractures (diffuse recharge area A_s) are 92% of the epikarst zone. Additionally, precipitation can indirectly recharge into the fast reservoir through sinkholes in the depression by collecting the lateral surface/subsurface flow (defined as concentrated recharge). Previous studies indicated that only when the precipitation amount in a heavy rainfall event (per day) exceeds a critical threshold of 60mm (Peng et al., 2012), the lateral surface/subsurface flow occurs. Therefore, in this study, when the precipitation amount is lower than the threshold of 60mm, the recharge areas of slow and fast flow reservoirs (A_s and A_f) are set to 0.92A and 0.08A, respectively; when the rainfall amount is >60mm, A_f is equal to concentrated recharge area in terms of the identified sinkhole drainage areas (4.51, 9.43

and 15.5 km^2 for the (sub-) catchment of MZD, LHT and MSK, respectively), and the remaining areas are regarded as the recharge area A_s.

Although the multi-flows in a karst catchment exhibit significant nonlinearity, linear algorithms also can be used to characterize water and solute transport processes in simplified karst system (Charlier et al, 2012; Hartmann et al 2013). In order to simplify the calculation, the linear relation between the reservoir storage V and flow discharge Q (subscripts of s and f represent the slow and fast flow reservoirs, respectively) is assumed as:

$$V_{s,t} = k_s Q_{s,t} \tag{5}$$

$$V_{f,t} = k_f Q_{f,t} \tag{6}$$

where k_s and k_f are the constants reflecting the relation between storage and discharge of the slow and fast flow reservoirs, respectively. Inserting Eqs (5) and (6) into Eqs (3) and (4) obtains:

$$Q_{s,t} = \frac{1}{k_s + \frac{fk_s}{k_e}\Delta t}\left(I_{s,t}\Delta t + k_s Q_{s,t-1} + \frac{k_f Q_{f,t}}{k_e}\Delta t\right) \tag{7}$$

$$Q_{f,t} = \frac{\Delta t}{k_f + \frac{k_f}{k_e}\Delta t + \Delta t} I_{f,t} + \frac{k_f}{k_f + \frac{k_f}{k_e}\Delta t + \Delta t} Q_{f,t-1} + \frac{fk_s \Delta t Q_{s,t}}{k_e\left(k_f + \frac{k_f}{k_e}\Delta t + \Delta t\right)} \tag{8}$$

Eqs (7) and (8) can be expressed as following general forms of linear equations:

$$Q_{s,t} = \Phi_{s,1} I_{s,t} + \Phi_{s,2} Q_{s,t-1} + \Phi_{s,3} Q_{f,t} \tag{9}$$

$$Q_{f,t} = \Phi_{f,1} I_{f,t} + \Phi_{f,2} Q_{f,t-1} + \Phi_{f,3} Q_{s,t} \tag{10}$$

where $\Phi_{s,n}$ and $\Phi_{f,n}$ are coefficients of the equations associated with reservoir parameters of k_s and k_f, and the time interval Δt (Appendix A).

Solution of Eqs (9) and (10) requires observational data of flow discharges in the slow and fast reservoirs, as well as the recharge rates. However, at most sites (e.g. Houzhai catchment), only flow discharge is observed at outlets of underground channels and surface channels. Hence, we transferred Eqs. (9) and (10) into following iterating equations to remove the slow reservoir routing:

$$Q_{f,t} = a_0 I_{f,t} + b_0 I_{s,t} + b_1 I_{s,t-1} + b_2 I_{s,t-2} + \ldots\ldots + b_n I_{s,t-n} + d_1 Q_{f,t-1} + d_2 Q_{f,t-2} + \ldots\ldots + d_n Q_{f,t-n} + g_0 Q_{s,t-n} \quad (11)$$

where a_0, $b_0 \ldots b_n$, $d_1 \ldots d_n$, and g_0 are polynomial representations of $\Phi_{s,n}$ and $\Phi_{f,n}$ (Appendix A). The Eq (11) is an Auto-Regressive and Moving Average Model (ARMA), which can be used to simulate the flow discharge only using the outlet discharge (conduit flow).

In order to simulate discharge using the derived ARMA, time lag (n) or memory effect (t-n) of the catchment fractures and conduits on the catchment outflow in Eq (11) needs to be determined in advance. Based on discharge time series, the time lag can be identified by the partial autocorrelation function (PACF). High memory indicates a poorly developed karstic network and slow response of rainfall-outlet flow discharge. In contrast, low memory reflects highly karstified aquifer and fast response of rainfall- outlet flow discharge (Mangin, 1971).

3.2 Hydrochemical module of dissolved Ca and Mg released to streamflow

The chemical mass balance of carbonate rock dissolution in the slow and fast flow reservoirs can be expressed as:

$$\frac{dC_{s,t}V_{s,t}}{dt} = C_{p,t}I_{s,t} + Rate_{s,t} + \frac{C_{f,t}V_{f,t} - fC_{s,t}V_{s,t}}{k_e} \quad (12)$$

$$\frac{dC_{f,t}V_{f,t}}{dt} = C_{p,t}I_{f,t} + Rate_{f,t} - \frac{C_{f,t}V_{f,t} - fC_{s,t}V_{s,t}}{k_e} - C_{f,t}Q_{f,t} \quad (13)$$

where $C_{s,t}$ and $C_{f,t}$ are concentrations of chemical components in the slow and fast flow reservoirs, respectively. $C_{p,t}$ is the concentration of chemical components from the infiltrated rainfall (4.5mg/L by Yu, 1990). $Rate_{s,t}$ and $Rate_{f,t}$ are contribution from other sources, e.g. the carbonate reaction and weathering in the slow and fast flow reservoirs, respectively.

A linear relationship between the storage mass *CV* and the transport *CQ* is assumed as:

$$C_{s,t}V_{s,t} = k_s C_{s,t}Q_{s,t} \quad (14)$$

$$C_{f,t}V_{f,t} = k_f C_{f,t}Q_{f,t} \quad (15)$$

Inserting Eqs (14) and (15) into Eqs (12) and (13) obtains:

$$C_{s,t}Q_{s,t} = \frac{1}{k_s + \frac{fk_s}{k_e}\Delta t}\left(C_{p,t}I_{s,t}\Delta t + Rate_{s,t}\Delta t + k_s C_{s,t-1}Q_{s,t-1} + \frac{k_c C_{f,t}Q_{f,t}}{k_e}\Delta t\right) \quad (16)$$

$$C_{f,t}Q_{f,t} = \frac{\Delta t}{k_f + \frac{k_f}{k_e}\Delta t + \Delta t}C_{p,t}I_{f,t} + \frac{k_f}{k_f + \frac{k_f}{k_e}\Delta t + \Delta t}C_{f,t-1}Q_{f,t-1} + \frac{fk_s\Delta t C_{s,t}Q_{s,t}}{k_e(k_f + \frac{k_f}{k_e}\Delta t + \Delta t)} + \frac{\Delta t}{k_f + \frac{k_f}{k_e}\Delta t + \Delta t}Rate_{f,t} \quad (17)$$

Eqs (16) and (17) can be expressed as following general forms of linear equations.

$$C_{s,t}Q_{s,t} = \Psi_{s,1}C_{p,t}I_{s,t} + \Psi_{s,2}C_{s,t-1}Q_{s,t-1} + \Psi_{s,3}C_{f,t}Q_{f,t} + \Psi_{s,4}Rate_{s,t} \quad (18)$$

$$C_{f,t}Q_{f,t} = \Psi_{f,1}C_{p,t}I_{f,t} + \Psi_{f,2}C_{f,t-1}Q_{f,t-1} + \Psi_{f,3}C_{s,t}Q_{s,t} + \Psi_{f,4}Rate_{f,t} \quad (19)$$

where $\Psi_{s,n}$ and $\Psi_{f,n}$ are coefficients shown in Appendix A.

Inserting Eq. (18) into (19), the iterating form of the chemical mass by catchment outlet flow is expressed as:

$$C_{f,t}Q_{f,t} = A_0C_{p,t}I_{f,t} + B_0C_{p,t}I_{s,t} + B_1C_{p,t-1}I_{s,t-1} + \ldots\ldots + B_nC_{p,t-n}I_{s,t-n} + D_1C_{f,t-1}Q_{f,t-1} + \ldots\ldots + D_nC_{f,t-n}Q_{f,t-n} + g_0C_{s,t-n}Q_{s,t-n} + E_0Rate_{f,t} + F_0Rate_{s,t} + F_1Rate_{s,t-1} + \ldots\ldots + F_nRate_{s,t-n} \quad (20)$$

where A_0, $B_0 \ldots B_n$, $D_1 \ldots D_n$, G_0, E_0 and $F_1 \ldots F_n$ are polynomial representations of $\Psi_{s,n}$ and $\Psi_{f,n}$ (Appendix A).

Calcite dissolution occurs by reaction in the system between carbon dioxide (CO_2), water (H_2O) and calcite ($CaCO_3$). The presence of CO_2, either in the soil or dissolved from the atmosphere enhances calcite dissolution by generating additional acidity in the aqueous solution. Therefore, precipitation recharge has an important role in the formation of dissolution features (Lakshmanan et al, 2003; Dar et al, 2015). Meanwhile, when there is active flow from the precipitation recharge, the groundwater will become under-saturated with respect to $CaCO_3$ (Worthington, 2003), which further enhances the potential for dissolution. Therefore, the rate of the carbonate dissolution *Rate* is assumed as non-linear proportional to the recharge rate I_s and I_f:

$$Rate = D + (a + bX^2)^{\frac{1}{2}} \quad (21)$$

where D, a and b are constants, X is either I_s for $Rate_s$ or I_f for $Rate_f$. The model parameters are illustrated in Table 1.

3.3 Modelling procedure

The ARMA form of Eqs (11) and (20) for the flow discharge and solution, respectively, is beneficial for determining the parameters in relation to the observed series of discharge and concentration. The model parameters are calibrated as follows: (1) the parameters primarily dependent on rock fracture structure (e.g. f) and dissolution of soluble rock (a, b and D), which are relatively stable in a long-term period. These parameters were calibrated by using the observation data during the whole period from 1 January 1997 to 31 December 2001; (2) the parameters dependent on flow discharge (k_s, k_f, k_e, α and β), which most likely arise from the non-linear relation of the storage-discharge and precipitation-recharge due to catchment heterogeneity. These parameters were calibrated separately to the observations in individual years to reflect inter-annual climatic variation.

The modified Kling–Gupta efficiency (KGE) criterion (Kling et al.,2012) was used as the objective function for calibration in this study. The KGE is a three dimensional representation (Euclidean distance) of the widely used Nash–Sutcliffe criterion overcoming some weaknesses of the latter (Schaefli and Gupta, 2007) balancing dynamics (correlation coefficient), bias (bias ratio) and variability (variability ratio). In this study, flow discharge and chemical concentration were combined to formulate a single objective function, as $KGE_j = (KGE_d + KGE_c)/2$ (KGE_d is for discharge, KGE_c is for solute concentration). A Monte Carlo approach was used to explore a suitable range of the parameter space. The range of some parameters closely related to catchment characteristics may be very different for the different sites. In order to derive a more behavioural parameter set, two calibration iterations

were carried out. First, a total of 10^5 different parameter combinations were tested. And then, the parameter ranges were reduced according to the best models for the second calibration for different sites. This resulted in testing a total of 10^6 different parameter combinations.

4 Results

4.1 Variability of flow discharge and dissolved calcium and magnesium

Mean annual discharges are 0.13, 0.29 and 1.12 m^3/s (1997–2001), and the Ca+Mg concentrations are 86.8, 89.2 and 76.8mg/L at MZD, LHT and MSK, respectively. The rapid flow variability at the three sites is evident in terms of flow duration curves from the daily observation data during the period 1997–2001 (Figure 3). The east mountainous area at MZD, rich in sinkholes linked with the underground channels, has the sharpest rise and decline of the hydrograph. When the underground channel stretches to the broad and flat peneplains in the middle and downstream, underground flow attenuates and the flow duration curves become relatively smooth. The variability in the solute concentration is similar at the three sites although the mean solute concentration is lower at MZD (Figure 3).

Figure 4 shows the time-series of daily discharge and the Ca+Mg concentration in routine samples at the three stations. There is marked seasonality of both discharge and solute concentrations over the study period, with solute concentrations at all three stations being negatively correlated with discharges.

Summary statistics for precipitation, discharge and concentration of Mg^{2+}+Ca^{2+} during the wet and dry seasons at the three stations are shown in Table 2. Higher discharges correspond with lower concentrations in the wet season, and lower discharges correspond

with higher concentrations in the dry season. Spatially, concentration decreases as discharge increases from the upper catchment of MZD to the outlet of MSK (discharge vs. concentration at the three stations in Table 2). However, the solute flux or transport mass QC is more strongly proportional to discharge, higher in wet season and at the downstream and lowest in the dry season and at the upstream site.

4.2 Modelling results

(1) Model verification

The partial autocorrelation function (PACF) gives the partial correlation of a time series with its own lagged values, where there is no dependence on intermediate elements within the lag. PACF values reveal dependence between observations on the outflow discharge time series resulting from karstic aquifer "memory". Hence, it is a tool for identifying some overall characteristics of the discharge time series, particularly cyclic variations. The PACF was calculated on the basis of daily outflow discharge of 1997–2001 at the three stations (Figure 4). The time required for the correlogram to drop below 0.2 reflects the "memory effect" (Mangin 1971), which means the conduit system has less influence on the outflow. Hence, the time-lags (n in Eqs (11) and (20)) at the three stations are ~2 days based on the values of PACF in Figure 4.

The parameter ranges are listed in Table 3. For the analysis, the behavioural parameter sets were retained from the best 500 runs, which were applied to simulate model outputs. This provides a range of accepted models which gives a first approximation of the model uncertainty in lieu of a more formal uncertainty analysis (Birkel et al., 2015). The model

results show that the discharge and concentration dynamics are mostly captured by the simulation ranges at the three stations; and though some peak discharges were underestimated (Figure 5). The objective function value of KEG_j at the three stations is all greater than 0.65 for the best 500 parameter sets (Table 3). The performance of the model is best at MSK with the KEG_j greater than 0.75 in each water year and worst at MZD with KEG_j of 0.65. As is common in coupled flow-tracer models, the performance in the simulation of Mg+Ca is more uncertain than for discharge at the three stations, with KEG_d ~0.8 compared with ~0.6 for KEG_c.

(2) The calibrated parameters

Table 3 lists the mean parameter values derived from the best 500 parameter sets after the second round of calibration (with the highest KGE_j) and gives insight into the process conceptualisation from the calibrated model. The parameters of k_s and k_f (ratio of storage to discharge) reflect the response of flow in slow and fast flow reservoirs to respective reservoir storage. These parameters can be used to assess the hydraulic turnover times of the study sites and can be used to estimate the system's regulation of groundwater. The calibrated values of k_s and k_f increase from upstream to downstream, e.g. 30 and 1 days at MZD and 96 and 39 days at MSK for k_s and k_f, respectively. It indicates that the high gradient of the mountainous areas and strong connections of fracture and channel networks in the upstream area at MZD leads to the storage being rapidly flushed and hence the short turnover time. This result is consistent with the statistical results from typical karstic springs by Zhang et.al. (2013).

Temporal variability of k_f is related to precipitation/discharge variation. As shown in

Figure 6, k_f calibrated in each of the years at MSK and LHT is inversely correlated with annual rainfall, although uncertainty exists due to the short observation series. There is no obvious difference in hydraulic turnover time for MZD in each year because of the short response time of discharge to storage (just 1 day). The precipitation/discharge dependent mean hydraulic turnover time ($k_f = V_{f,t} / Q_{f,t}$) most likely arises from a non-linear storage-discharge relationship due to the heterogeneity of conduit structure. As water table is lower in drier years, k_f is higher under gentler hydraulic gradients since the conduits/channels are well developed in the lower aquifer above the bedrock. In contrast, when the water table is higher in wetter years, k_f becomes smaller under a steeper hydraulic gradient since conduits/channels are less well-developed in the higher aquifer. Thus, the mean hydraulic turnover time k_f is longer in drier years than wetter years.

The k_e parameter represents the duration of flow exchange between the fast and slow reservoirs, and f is the ratio of porosity of the connection between them. As the network connectivity decreases from the upstream to the downstream, the ratio of porosity of the quick to slow flow reservoir decreases (f in Table 3) and thus duration of the flow exchange becomes longer (k_e in Table 3) attenuating the hydrograph.

The coefficient of precipitation recharge into slow flow reservoir α is lower than the coefficient of the fast flow reservoir β because the infiltration rate in soils and fractures is slower than that in conduit and channel, and thus more water remains in the soils and fractures for evaporation loss. Both α and β decrease from the headwaters to the outlet as less evaporation and more precipitation recharge in the headwater areas with the thinner soil and

denser conduits and sinkholes, compared with the downstream agriculture areas occupied by mostly flatter areas with thicker soils.

The parameters of a, b and D determine the rate of the carbonate dissolution by active flow from the precipitation recharge in the critical zone. b, as the rate of the carbonate dissolution for unit rainfall recharge, is the most sensitive parameter. The calibrated values of b decrease from upstream to downstream, which indicates that the dissolution capacity by the recharge water reduces possibly due to the decrease of the ratio of CaO/MgO for the limestone, but also the increase of the duration of flow exchange between the fast and slow reservoirs from upstream to downstream.

In order to test the resulting models, we run the model in each year using the best 500 parameter sets for each other year similar to Soulsby et al. (2016). Overall, the parameters transfer well across the years in terms of maintaining reasonable KGE_i scores. For example, at the headwater of MZD, the highest KGE_j in years of 1998~ 2001, with the best 500 parameter sets for 1997, are 0.66, 0.57, 0.54 and 0.60, respectively (Table 4). The results show that highest KGE_j at the three outlets are usually higher than 0.60, indicating simulation of water and mass transport is generally reliable in the catchment.

(3) Exchange between the fast and slow flow systems

The exchange fluxes between the fast and slow flow systems (Q_E) were calculated using Eq (2) in the three monitored catchments. The modelled positive and negative value in Figure 7 illustrates water storage in the matrix/fractures draining into conduits and then being recharged by water in conduits, respectively. Obviously, there is bi-directional

exchange between the two systems. During the dry season, as water table levels in the conduits and underground channels drop more rapidly than in the fractures, water stored in the fractures mostly drains into conduits and channels as baseflow. In the wet season, especially during the periods of high flow, infiltrated water quickly fills conduits where water table is higher than the adjacent fractures. Water temporarily stored in the conduits, hence recharges the fractures. This bidirectional flow exchange is a unique feature of karstic areas.

Modelled differences in the exchange flows at the three stations are consistent with the contrasting nature of the fracture-conduit network at the three different scales. The results show that the amounts of bi-directional flow exchange increase from headwater to outfall. However, during dry periods, MZD has the largest proportion of positive flow exchange in the total discharge (87.5% for MZD, 70% for LHT and 64.1% for MSK), indicating the lower storage capacity of the conduit and channel networks and greater hydraulic gradient between the two reservoirs in the headwaters. Meanwhile, volumes of negative flow exchange are very small. Periods when drainage of stored water is greater than recharge from the fractures correspond to prolonged dry periods, and the ecosystem in the headwater where storage is more limited is more vulnerable to the shortage of water resources. In the wet season, MZD has the lowest proportion of negative flow exchange in the total discharge (6.4% for MZD, 16.8% for LHT and 35% for MSK) corresponding to the low hydraulic turnover. Thus, the underground channel network and lower gradients in the middle and lower catchment provide larger contact area for exchange between the quick and slow flow system for flow exchange. This also explains the more dramatic changes in hydrograph in headwaters and the

subsequent attenuation downstream (Figure 3).

The migration of Ca+Mg between fast and slow flow systems was simulated and the mean mass exchange (CQ) were calculated in the three catchments. As the mass exchange is driven by the water fluxes, solutes in the fractures migrates into and out the conduit system in the dry and wet seasons, respectively (Figure 8), behaving similar with the flow exchange. During the dry season, a large proportion of the total mass export at the outlet is mobilized from the matrix and fractures draining into the conduits (shown as positive in Fig 9). This proportion decreases from the headwaters to the lower catchment (81.7% for MZD, 57.1% for LHT and 43.4% for MSK). However, in wet season, the proportion of negative mass exchange from the conduit to fracture system in the total mass export at the outlet increases downstream (2.1% for MZD, 9.2% for LHT and 24.6% for MSK). This indicates that the well-developed channel network with a lower gradient in the critical zone of the middle and lower catchment regulates the dual flow system's control on solute as well as groundwater fluxes.

In contrast to the variability of flow exchange where positive variation is more marked than the negative (Fig 8), positive mass exchange variation is less than the negative exchange (Fig 9). The disparity arises from the lower difference in the concentration between fractures and conduits due to strong mixing of water sources by the frequent flow exchanges in the wet season.

(4) Source contributions of flow and mass transport at the catchment outlet

The catchment outflow at the time t, $Q_{f,t}$, is generated by precipitation recharge through

conduits and sinkholes $I_{f,t}$, previous conduit flow $Q_{f,t-1}$ and fracture flow $Q_{E,t}$, as described by Eq (A8); the model allows us to estimate the dynamics of these fluxes. Contribution of $Q_{E,t}$ is estimated by flow exchange from fractures to conduits (positive value in Fig 8). Contributions of different sources to the catchment outflow changes with rainfall amount and the ratio of contribution from the sources in headwater MZD is different to those in the lower catchments of LHT and MZD (Figure 9). In the headwater at MZD, the largest contribution is from $I_{f,t}$, which rapidly increases with daily precipitation amounts up to ~40 mm and then remains relative stable contributing almost all flow. The ratio change is related to the high density of sinkholes that collect surface/subsurface flow into underground channels which initially increases dramatically with precipitation. The ratios from the slow flow system ($Q_{E,t}$) and the antecedent fast flow system ($Q_{f,t-1}$) remain similar, but decrease with precipitation.

In the lower catchments at LHT and MZD, the largest contribution is from $Q_{f,t-1}$ and then becomes $I_{f,t}$ as precipitation amounts exceed a critical value (e.g. ~20mm for LHT and >80mm for MSK). The slow flow from fractures ($Q_{E,t}$) accounts for only a small fraction of the outlet flow, which can be only distinguished in the extremely small rainfall events or at baseflows. The higher fraction of the antecedent fast flow contribution ($Q_{f,t-1}$) in the downstream catchments indicates that catchment regulation by the sub-surface channel networks becomes stronger.

The ratio of these antecedent fast flow contributions ($Q_{f,t-1}$) decreases with daily precipitation amount while precipitation recharge through conduits and sinkholes $I_{f,t}$ increases. This indicates that “new” water recharge displaces the previous remaining “old water” during

the event.

The mass export of Ca+Mg is transported by the three conceptual flow components ($C_pI_{f,t}$, $C_{f,t-1}Q_{f,t-1}$, and $C_{s,t}Q_{E,t}$) and mobilized by dissolution in the conduits $Rate_{f,t}$, which were calculated using Eq (A9) . The results in Figure 9 show that contribution to the solute flux by the precipitation recharge ($C_pI_{f,t}$,) is very low because of the low concentration of rain water although the volumetric contribution of precipitation recharge ("new" water) to flows is much larger. As the low concentration "new" water recharges into underground channel, it accelerates dissolution of carbonate rocks ($Rate_{f,t}$) and reducing the relative contributions the mass transport by previous conduit flow ("old" water, $C_{f,t-1}Q_{f,t-1}$) and fracture flow ($C_{s,t}Q_{E,t}$), particularly at MZD.

As the precipitation recharge $I_{f,t}$ contributes the largest flow component but the lowest concentration in the outlet flow in the headwater MZD, dissolution of carbonate rocks ($Rate_{f,t}$) becomes the dominant source of total mass export. In the middle and downstream catchment, the effect of "new" water on the dissolution of carbonate rocks reduces. The mass transport by previous conduit flow ("old" water, $C_{f,t-1}Q_{f,t-1}$) makes the largest contribution to the total mass export for precipitation amount less than the critical threshold values of ~20mm for LHT and >80mm for MSK. The large, rapid contribution of dissolution of carbonate rocks ($Rate_{f,t}$) indicates that using as traditional mixing models with constant end-member compositions may lead to erroneous results due to solute uptake from water-rock interaction (i.e. $Rate_{f,t}$).

5 Discussion

Due to limited knowledge about the structure of subsurface drainage networks, hydrological models that only focus on the simulation of the hydrograph, are usually uncertain even if successful in flow simulations as they may "give the right answer for the wrong reason" (Kirchner, 2006) due to the common equifinality problem (Beven, 1993). In karst areas, the complex underground flow system which includes Darcy flow, fissure flow and channel/conduit flow, is a particular challenge to hydrological models. Hence, incorporating additional multi-proxy data (e.g. remote sensing, geophysical exploration or hydrochemial tracers) in hydrological models is important and potentially provides useful tools for constraining models. Tracers, linking hydrochemical processes and hydrodynamic conditions, can give integrated insights into the hydrological and geochemical functions of the karst critical zone. In karst areas in particular, geochemical tracers from different parts of the critical zone, (e.g. soil matrix/fractures and conduits) can be used to identify water sources, flow paths, residence times and mixing effects. Thus tracers are useful tools to test the results from hydrological models; here we simply provide a proof of concept, but there is much more potential to realise.

In the context of the Houzhai catchment, although a physically-based numerical groundwater model has previously been developed and applied successfully (Chen et al., 2013), it was based on the hypothesis of a conceptualized, equivalent continuous medium. This is unable to conceptualise a clear distinction of flow processes in karst critical zone because it does not separate the interaction of the fast and slow components of the flow system. Hence, the dual flow dynamics is the focus of this study because this is fundamental

to understanding the hydrological function of karst critical zone. Liu et al, (2010b) identified this issue based on the method (recession curve) by Mangin (1975) and developed the first conceptual model for dual flow in this watershed. However, they only focused on the spring hydrograph at the outlet and not internal catchment processes. The conductive capacity of the water drainage system was assumed to be sufficiently high to restrict any exchange and transient storage in the conduit network was ignored. But in the current study, we coupled a conceptual dual reservoir runoff model with an associated algorithms to assess dissolution rates in the "fast flow" and "slow flow" systems in three nested karst catchments with contrasting fissure-conduit networks. We found that the conduit network has substantial storage and can regulate groundwater fluxes, especially in the downstream area.

The focused recharge to underground channels through sinkholes has been widely identified by karst researchers. In the Houzhai catchment, the hydrological function of sinkholes were estimated by modelling the surface flow assumed to be captured by sinkholes (Meng et al, 2009) or calculation of the fast recharge to underground channels reflecting the sinkhole influence (Chen et al, 2008). However, these studies didn't include the dual flow systems and were based on the assumption that the influence of sinkholes is constant; here we show that the contribution of direct infiltration to the underground channel ($I_{f,t}$ in Eq (4)) varies with rainfall (Figure 8). Our ARMA type model derived from the conceptual model for dual flow systems of karst area developed by Hartmann et al (2013) enhances capacity in identifying catchment memory effects by using time series analysis of PACF. In addition, our model can take into account sinkhole effects on concentrated recharge and thus reasonably

captures the rapid rise and decline of the hydrograph. For solute transport simulation, our model also has the capacity to describe the relationship between dissolution rate and discharge in comparison to the constant contribution of solute used by Hartmann et al, (2013).

Furthermore, there has been no previous coupled model of flow and solute transport in this catchment, and we provide a simple, coupled conceptual model for flow and solute transport in the karst critical zone. For the hydrochemical component of the model, although a simple empirical relationship was used, the algorithm captures the main weathering process of carbonate in fracture and conduit networks. The result of the modelled mean annual flux of dissolved Ca and Mg in the Houzhai catchment (about 2847 t/yr) is comparable to the result calculated by observation data (CQ, in Table 2, is about 2712 t/yr) and other studies in the catchment. According to Yan et al (2011), the mean annual carbon uptake was 9.8 ± 2.1 g C m^{-2} yr^{-1} for underground water in Houzhai catchment. Based on the chemical formulas of $CaCO_3 + H_2O + CO_2 \Leftrightarrow Ca^{2+} + 2HCO_3^-$ and $MgCO_3 + H_2O + CO_2 \Leftrightarrow Mg^{2+} + 2HCO_3^-$, the amount of dissolved Ca and Mg is between 1441±309 (only for magnesium carbonate, $MgCO_3$) and 2401±515 tons (only has calcium carbonate, $CaCO_3$) in one year in the whole catchment. Thus, despite the simplifications employed, the model yields useful insights that improve our generic understanding of the hydrological and hydrochemical processes and associated controls for karst critical zones. Furthermore, we present a framework that could be used to project the potential consequences of future climatic and land use change on discharge and the solute composition of waters draining karst

catchments with different characteristics.

Exchange of groundwater between the fracture matrix and conduits is governed by differences in hydraulic head as well as the hydraulic conductivities between the two flow systems. Some previous studied have used numerical models to simulate such exchange (Kaufmann and Braun, 2000; Bauer and Sauter, 2003, Chen et al, 2012). However, most of these models are theoretical or based on experiments rather than practical application at the catchment-scale karst, because of the difficulty of observation in field. Bailly-Comte et al (2010) estimated the exchange of groundwater between the fracture matrix and conduits in one karst aquifer in north-central Florida (USA) using the water balance equation. However, this method is difficult to use elsewhere, because it was developed for sinking streams on the karst aquifer and the direct observation data of allogenic recharge. In addition, geochemical tracers were used to estimate the exchange in the same aquifer, although this focused on individual wells, and therefore may not characterise the exchange in a heterogeneous aquifer. In comparison, we provide a generic conceptual approach for quantifying the exchange of groundwater between fracture matrix and conduits that is scale independent and transferable because of the simple model structure and limited input data needed. Our study illustrates regional characteristics of the model parameters and the estimated flux of bidirectional flow and solute exchange between the fissure and conduit system presents, such as the flux increases from the headwaters to the outfall due to the large area of the developed conduits and low hydraulic gradient in the lower catchment.

Such quantitative assessment of water sources in karst environments is also

fundamentally important to ecosystem protection. Our work here shows that traditional methods of using end member mixing to estimate the volumetric contributions that different water sources make to stream flow over the year is severely compromised in karst areas, because of the multi-phase nature of the porous medium, together with confounding effects of different soil cover, land use and human activities. Thus it is difficult to characterise all the end-member compositions; for example, end-members in fine fissures are usually difficult, if not impossible, to sample. The model developed here provides a useful alternative method to quantify the volumetric contributions of water sources to underground channel, although it simplifies the water sources to three generic types which reflect the main underground flow processes. Of course such lumped conceptual models provide no explicit insight into the spatial distribution of processes within each catchment, but the nested approach here gives some sense of the changing process dominance with scale and how it affects stream flow response and the solute composition. This emphasises the key role of underground channels and sinkholes, which remains crucial science questions in the hydrology of the karst critical zone.

6 Conclusions

In this study, we developed a conceptual flow-tracer model that combines a dual reservoir runoff model with an ARMA model for the karst critical zone. We calibrated the model on both flows and solute concentrations to show how flow exchange between fissure and conduit networks changes in relation to catchment storage dynamics in three nested karst catchments. The aquifer in the lower catchment exerts a strong influence on fluxes of water

and mass of solute in the sub-surface due to the large area of the developed conduits and significant exchange flows between the matrix and conduit. According to the model results, rainfall amounts have a significant influence on partitioning the relative proportions of flow and solute from different source reaching the underground outlet. Additionally, the structure of the karst critical zone, e.g. epikarst and sinkholes, strengthen the effects of rainfall on catchment function. Thin epikarst and well-developed sinkholes in the headwater catchment diverts more surface water (younger water) into the underground channel network, leading to the sharp changes in hydrography and solute concentration.

This model is, however, only tested on outlet flow discharge and chemical mass. The details of source contributions of the flow and mass transport need to be further investigated in the model, e.g. infiltration and mass transport functions in the epikarst zone, and model validation still relies on more detail observation data of the various hydrological and chemical processes.

Acknowledgments

This research was supported by The UK-China Critical Zone Observatory (CZO) Programme (41571130071), the National Natural Scientific Foundation of China (41571020), National 973 Program of China (2015CB452701) and the Natural Environment Research Council (NE/N007425/1).

Appendix A

Flow routing:

According to Eq. (9), the $Q_{s,t}$ at previous time intervals (e.g. a two-time interval) can be expressed as:

$$Q_{s,t-1} = \Phi_{s,1} I_{s,t-1} + \Phi_{s,2} Q_{s,t-2} + \Phi_{s,3} Q_{f,t-1} \quad \text{(A1)}$$

$$Q_{s,t-2} = \Phi_{s,1} I_{s,t-2} + \Phi_{s,2} Q_{s,t-3} + \Phi_{s,3} Q_{f,t-2} \quad \text{(A2)}$$

Inserting Eqs (A1) and (A2) into Eq. (9) obtains:

$$Q_{s,t} = \Phi_{s,1} I_{s,t} + \Phi_{s,2}\Phi_{s,1} I_{s,t-1} + \Phi_{s,2}^2 \Phi_{s,1} I_{s,t-2} + \Phi_{s,2}^3 Q_{s,t-3} + \Phi_{s,2}^2 \Phi_{s,3} Q_{f,t-2} + \Phi_{s,2}\Phi_{s,3} Q_{f,t-1} + \Phi_{s,3} Q_{f,t} \quad \text{(A3)}$$

For the n time-lag intervals:

$$Q_{s,t} = \Phi_{s,1} I_{s,t} + \Phi_{s,2}\Phi_{s,1} I_{s,t-1} + \Phi_{s,2}^2 \Phi_{s,1} I_{s,t-2} + \ldots\ldots + \Phi_{s,2}^n \Phi_{s,1} I_{s,t-n} + \Phi_{s,2}^n Q_{s,t-n} + \Phi_{s,3} Q_{f,t} + \Phi_{s,2}\Phi_{s,3} Q_{f,t-1} + \Phi_{s,2}^2 \Phi_{s,3} Q_{f,t-2} + \ldots\ldots + \Phi_{s,2}^n \Phi_{s,3} Q_{f,t-n} \quad \text{(A4)}$$

Then, inserting Eq (A4) into (10) gives:

$$Q_{f,t} = \Phi_{f,1} I_{f,t} + \Phi_{f,2} Q_{f,t-1} + \Phi_{f,3}(\Phi_{s,1} I_{s,t} + \Phi_{s,2}\Phi_{s,1} I_{s,t-1} + \Phi_{s,2}^2 \Phi_{s,1} I_{s,t-2} + \ldots\ldots + \Phi_{s,2}^n \Phi_{s,1} I_{s,t-n} + \Phi_{s,2}^n Q_{s,t-n} + \Phi_{s,3} Q_{f,t} + \Phi_{s,2}\Phi_{s,3} Q_{f,t-1} + \Phi_{s,2}^2 \Phi_{s,3} Q_{f,t-2} + \ldots\ldots + \Phi_{s,2}^n \Phi_{s,3} Q_{f,t-n}) \quad \text{(A5)}$$

or :

$$(1 - \Phi_{f,3}\Phi_{s,3}) Q_{f,t} = \Phi_{f,1} I_{f,t} + \Phi_{f,2} Q_{f,t-1} + \Phi_{f,3}\Phi_{s,1} I_{s,t} + \Phi_{f,3}\Phi_{s,2}\Phi_{s,1} I_{s,t-1} + \Phi_{f,3}\Phi_{s,2}^2 \Phi_{s,1} I_{s,t-2} + \ldots\ldots + \Phi_{f,3}\Phi_{s,2}^n \Phi_{s,1} I_{s,t-n} + \Phi_{f,3}\Phi_{s,2}^n Q_{s,t-n} + \Phi_{f,3}\Phi_{s,2}\Phi_{s,3} Q_{f,t-1} + \Phi_{f,3}\Phi_{s,2}^2 \Phi_{s,3} Q_{f,t-2} + \ldots\ldots + \Phi_{f,3}\Phi_{s,2}^n \Phi_{s,3} Q_{f,t-n} \quad \text{(A6)}$$

If catchment memory becomes insignificant at the time-lag of n, the items with the time-lag longer than n can be ignored. Then, we can obtain the linear forms of flow discharge as Eq.(11). In order to estimate the various flows to catchment outlet, we deduced the derivations as below. Inserting Eqs (5) and (6) into Eq. (2) obtains:

$$Q_{E,t} = -\frac{k_f Q_{f,t} - f k_s Q_{s,t}}{k_e} \tag{A7}$$

According to the concept model, the underground channel flow at outlet are generated by flow infiltrating through conduits, previous conduit flow and exchange flow between the two flow systems. Hence, we deduce the form of $Q_{f,t}$ associated with these items above by inserting Eq (A7) into Eq (8):

$$Q_{f,t} = \frac{k_e \Delta t}{k_e k_f + k_f \Delta t + k_e \Delta t} I_{f,t} + \frac{k_e k_f}{k_e k_f + k_f \Delta t + k_e \Delta t} Q_{f,t-1} + \frac{k_e \Delta t}{k_e k_f + k_f \Delta t + k_e \Delta t} Q_{E,t} \tag{A8}$$

The explanations of coefficients in Eqs (9) to (11) are:

$$\Phi_{s,1} = \frac{\Delta t}{k_s + \frac{f k_s}{k_e} \Delta t}, \quad \Phi_{s,2} = \frac{k_s}{k_s + \frac{f k_s}{k_e} \Delta t}, \quad \Phi_{s,3} = \frac{k_f \Delta t}{k_s k_e + f k_s \Delta t}$$

$$\Phi_{f,1} = \frac{\Delta t}{k_f + \frac{k_f}{k_e} \Delta t + \Delta t}, \quad \Phi_{f,2} = \frac{k_f}{k_f + \frac{k_f}{k_e} \Delta t + \Delta t}, \quad \Phi_{f,3} = \frac{f k_s \Delta t}{k_e (k_f + \frac{k_f}{k_e} \Delta t + \Delta t)}$$

$$a_0 = \frac{\Phi_{f,1}}{1 - \Phi_{f,3} \Phi_{s,3}}$$

$$b_0 = \frac{\Phi_{f,3} \Phi_{s,1}}{1 - \Phi_{f,3} \Phi_{s,3}}, \quad b_1 = \frac{\Phi_{f,3} \Phi_{s,2} \Phi_{s,1}}{1 - \Phi_{f,3} \Phi_{s,3}}, \quad b_2 = \frac{\Phi_{f,3} \Phi^2_{s,2} \Phi_{s,1}}{1 - \Phi_{f,3} \Phi_{s,3}}, \quad b_n = \frac{\Phi_{f,3} \Phi^n_{s,2} \Phi_{s,1}}{1 - \Phi_{f,3} \Phi_{s,3}},$$

$$d_1 = \frac{\Phi_{f,2} + \Phi_{f,3} \Phi_{s,2} \Phi_{s,3}}{1 - \Phi_{f,3} \Phi_{s,3}}, \quad d_2 = \frac{\Phi_{f,3} \Phi^2_{s,2} \Phi_{s,3}}{1 - \Phi_{f,3} \Phi_{s,3}}, \quad d_n = \frac{\Phi_{f,3} \Phi^n_{s,2} \Phi_{s,3}}{1 - \Phi_{f,3} \Phi_{s,3}}$$

$$g_0 = \frac{\Phi_{f,3}\Phi_{s,2}^n}{1 - \Phi_{f,3}\Phi_{s,3}}$$

Mass routing:

Similar to flow Eq (A8), the mass of chemical components by catchment outlet flow can be expressed as:

$$C_{f,t}Q_{f,t} = \frac{k_e\Delta t}{k_e k_f + k_f\Delta t + k_e\Delta t}(C_{p,t}I_{f,t} + Rate_{f,t}) + \frac{k_e k_f}{k_e k_f + k_f\Delta t + k_e\Delta t}C_{f,t-1}Q_{f,t-1} + \frac{k_e\Delta t}{k_e k_f + k_f\Delta t + k_e\Delta t}C_{E,t}Q_{E,t} \quad (A9)$$

When water storage flow from fracture to conduit system:

$$C_{E,t} = C_{s,t}$$

When water storage flow from conduit to fracture system:

$$C_{E,t} = C_{f,t}$$

The explanations of coefficients in Eqs (18) to (20) are:

$$\psi_{s,1} = \psi_{s,4} = \Phi_{s,1},\ \psi_{s,2} = \Phi_{s,2},\ \psi_{s,3} = \Phi_{s,3}$$

$$\psi_{f,1} = \psi_{f,4} = \Phi_{f,1},\ \psi_{f,2} = \Phi_{f,2},\ \psi_{f,3} = \Phi_{f,3}$$

$$A_0 = E_0 = a_0,\ B_0 = F_0 = b_0, \ldots.\ B_n = F_n = b_n$$

$$D_1 = d_1, \ldots.\ D_n = d_n,\ G_0 = G_0$$

The explanations of symbols in the Figure 2 are as fellows.

I_s and I_f are rainfall recharge into the slow flow reservoir and fast flow reservoir, respectively;

V_s and V_f are storage of slow and fast flow reservoir, respectively;

Q_s, and Q_f are outflow of slow and fast flow reservoir, respectively;

C_p, C_s and C_f are solute concentration of rainfall, slow and fast flow reservoir, respectively;

Q_e and C_e are exchange flow and solute concentration, respectively;

K_e, K_s and K_f are flow constant of exchange, slow and fast flow reservoir, respectively.

REFERENCES

Arfib B, Charlier JB. 2016. Insights into saline intrusion and freshwater resources in coastal karstic aquifers using a lumped Rainfall-Discharge-Salinity model (the Port-Miou brackish spring, SE France). Journal of Hydrology 540: 148–161 DOI: 10.1016/j.jhydrol.2016.06.010

Bonacci O. 1987. Karst hydrology, with Special Reference to the Dinaric Karst. DOI: PNR61

Bailly-Comte V, Martin JB, Jourde H, Screaton EJ, Pistre S, Langston A. 2010. Water exchange and pressure transfer between conduits and matrix and their influence on hydrodynamics of two karst aquifers with sinking streams. Journal of Hydrology 386 (1–4): 55–66 DOI: 10.1016/j.jhydrol.2010.03.005

Bauer S, Liedl R, Sauter M. 2003. Modeling of karst aquifer genesis: Influence of exchange flow. Water Resources Research 39 (10): n/a-n/a DOI: 10.1029/2003WR002218

Beven KJ. 1993. Prophecy, reality and uncertainty in distributed hydrological modelling. Advances in Water Resources. 16: 41–51

Birk S, Liedl R, Sauter M. 2006. Karst spring responses examined by process-based modeling. In Ground Water832–836. DOI: 10.1111/j.1745-6584.2006.00175.x

Birkel C, Soulsby C, Tetzlaff D. 2015. Conceptual modelling to assess how the interplay of hydrological connectivity, catchment storage and tracer dynamics controls nonstationary water age estimates. Hydrological Processes 29 (January 2015): 2956–2969 DOI: 10.1002/hyp.10414

Chang Y, Wu J, Jiang G, Kang Z. 2017. Identification of the dominant hydrological process and appropriate model structure of a karst catchment through stepwise simplification of a complex conceptual model. Journal of Hydrology DOI: http://dx.doi.org/10.1016/j.jhydrol.2017.02.050

Charlier J, Bertrand C, Mudry J. 2012. Conceptual hydrogeological model of flow and transport of dissolved organic carbon in a small Jura karst system. Journal of Hydrology 460–461: 52–64 DOI: 10.1016/j.jhydrol.2012.06.043

Chen N, Gunzburger M, Hu B, Wang X, Woodruff C. 2012. Calibrating the exchange coefficient in the modified coupled continuum pipe-flow model for flows in karst aquifers. Journal of Hydrology 414–415: 294–301 DOI: 10.1016/j.jhydrol.2011.11.001

Chen X, Chen C, Hao QQ, Zhang ZC, Shi P. 2008. Simulation of rainfall-underground outflow responses of a karstic watershed in Southwest China with an artificial neural network. Water Science and Engineering 1 (2): 1–9 DOI: 10.3882/j.issn.1674-2370.2008.02.001

Chen X, Zhang Y, Zhou Y, Zhang Z. 2013. Analysis of hydrogeological parameters and numerical modeling groundwater in a karst watershed, southwest China. Carbonates and Evaporites 28 (1–2): 89–94 DOI: 10.1007/s13146-013-0143-8

Dar FA, Perrin J, Ahmed S, Narayana AC, Riotte J. 2014. Hydrogeochemical characteristics of Karst Aquifer from a semi-arid region of Southern India and impact of rainfall recharge on groundwater chemistry. Arabian Journal of Geosciences: 2739–2750 DOI: 10.1007/s12517-014-1440-9

Field MS. 1993. Karst Hydrology and Chemical Contamination. Journal of Environmental Systems 22 (1): 1–26 DOI: 10.2190/X7MV-C93E-66GK-BFH7

Freeze RA, Cherry JA. 1979. Groundwater. Prentice-Hall, Englewood Cliffs, NJ, 604 pp

Ghasemizadeh R, Hellweger F, Butscher C, Padilla I, Vesper D, Field M, Alshawabkeh A. 2012. Review: Groundwater flow and transport modeling of karst aquifers, with particular reference to the North Coast Limestone aquifer system of Puerto Rico. Hydrogeology journal 20 (8): 1441–1461 DOI: 10.1007/s10040-012-0897-4

Hartmann A, Goldscheider N, Wagener T, Lange J, Weiler M. 2014. Karst water resources in a changing world: Approaches, of hydrological modeling. Review of Geophysics (1): 1–25 DOI: 10.1002/2013RG000443

Hartmann A, Wagener T, Rimmer A, Lange J, Brielmann H, Weiler M. 2013. Testing the realism of model structures to identify karst system processes using water quality and quantity signatures. Water Resources Research 49 (6): 3345–3358 DOI: 10.1002/wrcr.20229

Katz, Brian. Coplen, Tyler. Bullen, T. Hal Davis J. 1997. Use of Chemical and Isotopic Tracers to Characterize the Interations Between Ground Water and Surface Water in Mantled Karst. Ground Water 35 (6): 1014–1028 DOI: 10.1111/j.1745-6584.1997.tb00174.x

Kaufmann G, Braun J. 2000. Karst aquifer evolution in fractured, porous rocks. Water Resources Research 36 (6): 1381–1391 DOI: 10.1029/1999wr900356

Kirchner JW. 2006. Getting the right answers for the right reasons: Linking measurements, analyses, and models to advance the science of hydrology. Water Resources Research 42 (3) DOI: 10.1029/2005WR004362

Kling H, Fuchs M, Paulin M. 2012. Runoff conditions in the upper Danube basin under an ensemble of climate change scenarios. Journal of Hydrology 424–425: 264–277 DOI: 10.1016/j.jhydrol.2012.01.011

Ladouche B, Marechal JC, Dorfliger N. 2014. Semi-distributed lumped model of a karst system under active management. Journal of Hydrology 509: 215–230 DOI: 10.1016/j.jhydrol.2013.11.017

Lakshmanan E, Kannan R. 2003. Major ion chemistry and identification of hydrogeochemical processes of ground water in a part of Kancheepuram district, Tamil Nadu, India. Environmental Geosciences 10 (4): 157–166 DOI: 10.1306/eg100403011

Li SL, Liu CQ, Lang YC, Tao F, Zhao Z, Zhou Z. 2008. Stable carbon isotope biogeochemistry and anthropogenic impacts on karst ground water, zunyi, Southwest China. Aquatic Geochemistry 14 (3): 211–221 DOI: 10.1007/s10498-008-9033-4

Liu L, Shu L, Chen X, Oromo T. 2010b. The hydrologic function and behavior of the Houzhai underground river basin, Guizhou Province, southwestern China. Hydrogeology Journal 18 (2): 509–518 DOI: 10.1007/s10040-009-0518-z

Liu Z, Dreybrodt W, Wang H. 2010a. A new direction in effective accounting for the atmospheric CO2 budget: Considering the combined action of carbonate dissolution, the

global water cycle and photosynthetic uptake of DIC by aquatic organisms. Earth-Science Reviews 99 (3–4): 162–172 DOI: 10.1016/j.earscirev.2010.03.001

Mangin A. 1971. Etude des debits classes d'exutoires karstiques portent sur un cycle hydrologique. Annales de Spéléologie 28: 21–40

Mangin A. 1975. Contribution à l'étude hydrodynamique des aquifers karstiqus (Contribution to the hydrodynamic study of karst aquifers). Thèse Doctorat d' État ès Sciences, Univ. of Dijon, France Ann Spéléol 29(3):283–332; 29(4):495–601; 30(1):21–124

Meng HH, Wang LC, Su WC, Yu H. 2008. Development of karst sinkhole-based semi-distributed hydrological model and its application. SCIENTIA GEOGRAPHICA SINICA. 29(4): 550-554. (In Chinese)

Peng T, Wang SJ. 2012. Effects of land use, land cover and rainfall regimes on the surface runoff and soil loss on karst slopes in southwest China. Catena 90: 53–62 DOI: 10.1016/j.catena.2011.11.001

Pinault JL, Pauwels H, Cann C. 2001. Inverse modeling of the hydrological and the hydrochemical behavior of hydrosystems: Application to nitrate transport and denitrification. Water Resources Research 37 (8): 2179–2190 DOI: 10.1029/2001WR900017

Rimmer A, Hartmann A. 2012. Simplified Conceptual Structures and Analytical Solutions for Groundwater Discharge Using Reservoir Equations. Water Resources Management and Modeling 2: 217–238 DOI: 10.5772/34803

Ronayne MJ. 2013. Influence of conduit network geometry on solute transport in karst aquifers with a permeable matrix. Advances in Water Resources 56: 27–34 DOI: 10.1016/j.advwatres.2013.03.002

Quinlan JF, Ewers RO. 1985. Ground water flow in limestone terranes: strategy rationale and procedure for reliable, efficient monitoring of ground water quality in karst areas. 5th national symposium and exposition on aquifer restoration and ground water monitoring. National Water Well Association, Columbus, Ohio, pp 197–234

Schaefli B, Gupta H V. 2007. Do Nash values have value? Hydrological Processes 21 (15): 2075–2080 DOI: 10.1002/hyp.6825

Soulsby, C., Birkel, C. and Tetzlaff, D. 2016. Modelling storage-driven connectivity between landscapes and riverscapes: towards a simple framework for long-term ecohydrological assessment. Hydrological Processes 30:2482-2497.

Sugawara M. 1995. Tank model, Computer models of watershed hydrology, Singh, VP ed. Water Resources Publications, Colorado, pp. 165–214.

Sun A, Painter S, Green R. 2005. Modeling barton springs segment of the Edwards Aquifer using MODFLOW-DCM. In Geotechnical Special Publication.

White WB. 1988. Geomorphology and Hydrology of Karst Terrains. Oxford University Press, Oxford

White WB. 2007. Cave sediments and paleoclimate. Journal of Cave and Karst Studies 69 (1): 76–93

Worthington SRH. 2009. Diagnostic hydrogeologic characteristics of a karst aquifer (Kentucky, USA). Hydrogeology Journal 17 (7): 1665–1678 DOI: 10.1007/s10040-009-0489-0

Yan J, Li J, Ye Q, Li K. 2012. Concentrations and exports of solutes from surface runoff in Houzhai Karst Basin, southwest China. Chemical Geology 304–305: 1–9 DOI: 10.1016/j.chemgeo.2012.02.003

Yan J, Wang YP, Zhou G, Li S, Yu G, Li K. 2011. Carbon uptake by karsts in the Houzhai Basin, southwest China. Journal of Geophysical Research: Biogeosciences 116 (4) DOI: 10.1029/2011JG001686

Yang Y. 2001. A study on the structure of karst aquifer medium and the groundwater flow in Houzhai underground river basin. Carsologica Sinica 20(1):17-20. (In Chinese)

Yu JB, Yang LZ, Zhang HS, Fang MZ, Xing FM. 1990. The study of development regularity of karst in China - Water resources evaluation and exploitation in karst region in south of Puding in Guizhou Province. Science Press of China. (In Chinese).

Zhang Z, Chen X, Chen X, Shi P. 2013. Quantifying time lag of epikarst-spring hydrograph response to rainfall using correlation and spectral analyses. Hydrogeology Journal 21 (7): 1619–1631 DOI: 10.1007/s10040-013-1041-9

Zhang Z, Chen X, Ghadouani A, Shi P. 2011. Modelling hydrological processes influenced by soil, rock and vegetation in a small karst basin of southwest China. Hydrological Processes 25 (15): 2456–2470 DOI: 10.1002/hyp.8022

Zhao M, Zeng C, Liu Z, Wang S. 2010. Effect of different land use/land cover on karst hydrogeochemistry: A paired catchment study of Chenqi and Dengzhanhe, Puding, Guizhou, SW China. Journal of Hydrology 388 (1–2): 121–130 DOI: 10.1016/j.jhydrol.2010.04.034

Table 1 Description of the calibrated parameters

Coefficient	Units	Descriptions
K_s	day	The slow flow reservoir constant
K_f	day	The fast flow reservoir constant
k_e	day	Exchange constant between the two reservoirs
f	-	The ratio of porosity of the quick to slow flow reservoir
a	g^2/d^2	Dissolution constant
b	$g^2/(m^3)^2$	Dissolution constant
D	g/d	Stable solution amount
α	-	Precipitation recharge coefficient for slow flow reservoir
β	-	Precipitation recharge coefficient for fast flow reservoir

Table 2 Summary statistics of rainfall P, discharge Q, concentration C and mass export QC for MZD, LHT and MSK.

Stations	Period	P (mm)	Q (m^3/s)	C (mg/L)	QC (g/s)
MDZ	Dry season	219	0.013	93.1	1.2
	Wet season	1147	0.23	80.5	18.5
	Average	1366	0.13	86.8	11.3
LHT	Dry season	228	0.16	94.7	15.2
	Wet season	1157	0.42	83.7	35.2
	Average	1385	0.29	89.2	25.9
MSK	Dry season	307	0.70	84	58.8
	Wet season	1120	1.54	69.6	107.2
	Average	1427	1.12	76.8	86

Table 3 Mean parameter values and annual fitness derived from the best 500 parameter sets after calibration

MZD												
Coefficient	k_s	k_f	k_e	f	a	b	D (10^4)	α	β	KGE_d	KGE_c	KGE_j
Initial range	20-60	1-5	1-10	0.01-0.1	600-1200	1-2000	1-10	0-1	0-1	mean/best		
1997	22	1	1	0.07	948	1599	3	0.63	0.85	0.80/ 0.86	0.56/ 0.60	0.68/ 0.73
1998	27	1	3	0.07	948	1599	3	0.62	0.84	0.82/ 0.88	0.58/ 0.62	0.70/ 0.75
1999	33	1	2	0.07	948	1599	3	0.63	0.86	0.80/ 0.84	0.52/ 0.62	0.66/ 0.73
2000	33	1	3	0.07	948	1599	3	0.64	0.87	0.79/ 0.83	0.51/ 0.57	0.65/ 0.70
2001	36	1	5	0.07	948	1599	3	0.66	0.87	0.80/ 0.84	0.50/ 0.58	0.65/ 0.71
LHT												
Coefficient	k_s	k_f	k_e	f	a	b	D (10^4)	α	β	KGE_d	KGE_c	KGE_j
Initial range	20-60	1-10	5-15	0.01-0.1	600-1200	1-2000	1-10	0-1	0-1	mean/best		
1997	33	2	6	0.05	921	872	8.3	0.57	0.68	0.80/ 0.88	0.60/ 0.62	0.70/ 0.75
1998	37	3	7	0.05	921	872	8.3	0.54	0.7	0.81/ 0.87	0.57/ 0.59	0.69/ 0.73
1999	38	4	7	0.05	921	872	8.3	0.58	0.71	0.79/ 0.86	0.61/ 0.62	0.70/ 0.74
2000	38	4	7	0.05	921	872	8.3	0.59	0.68	0.81/ 0.88	0.51/ 0.56	0.66/ 0.72
2001	40	5	8	0.05	921	872	8.3	0.60	0.71	0.79/ 0.85	0.57/ 0.61	0.68/ 0.73
MSK												
Coefficient	k_s	k_f	k_e	f	a	b	D (10^6)	α	β	KGE_d	KGE_c	KGE_j
Initial range	50-150	20-60	30-80	0.01-0.1	600-1200	1-2000	1-10	0-1	0-1	mean/best		
1997	95	34	39	0.03	877	49	2.7	0.49	0.59	0.84/ 0.90	0.62/ 0.64	0.73/ 0.77
1998	96	39	59	0.03	877	49	2.7	0.46	0.59	0.83/ 0.88	0.59/ 0.62	0.71/ 0.75
1999	98	41	56	0.03	877	49	2.7	0.45	0.65	0.85/ 0.89	0.61/ 0.63	0.73/ 0.76
2000	-	-	-	-	-	-	-			-	-	-
2001	96	43	46	0.03	877	49	2.7	0.46	0.63	0.84/ 0.87	0.58/ 0.61	0.71/ 0.74

Table 4 Model results in each year using the best 500 parameter sets for other years

MZD	Best 500 parameter sets for				
	1997	1998	1999	2000	2001
1997	0.73	0.67	0.62	0.68	0.70
1998	0.66	0.75	0.64	0.61	0.68
1999	0.57	0.64	0.73	0.62	0.62
2000	0.54	0.57	0.51	0.70	0.58
2001	0.60	0.61	0.56	0.63	0.71
LHT	Best 500 parameter sets for				
	1997	1998	1999	2000	2001
1997	0.75	0.65	0.63	0.66	0.61
1998	0.70	0.73	0.71	0.66	0.70
1999	0.72	0.73	0.74	0.70	0.72
2000	0.55	0.62	0.65	0.72	0.58
2001	0.63	0.64	0.62	0.68	0.73
MSK	Best 500 parameter sets for				
	1997	1998	1999	2000	2001
1997	0.77	0.67	0.62	-	0.64
1998	0.66	0.75	0.73	-	0.70
1999	0.61	0.71	0.76	-	0.71
2000	-	-	-	-	-
2001	0.72	0.73	0.73	-	0.74

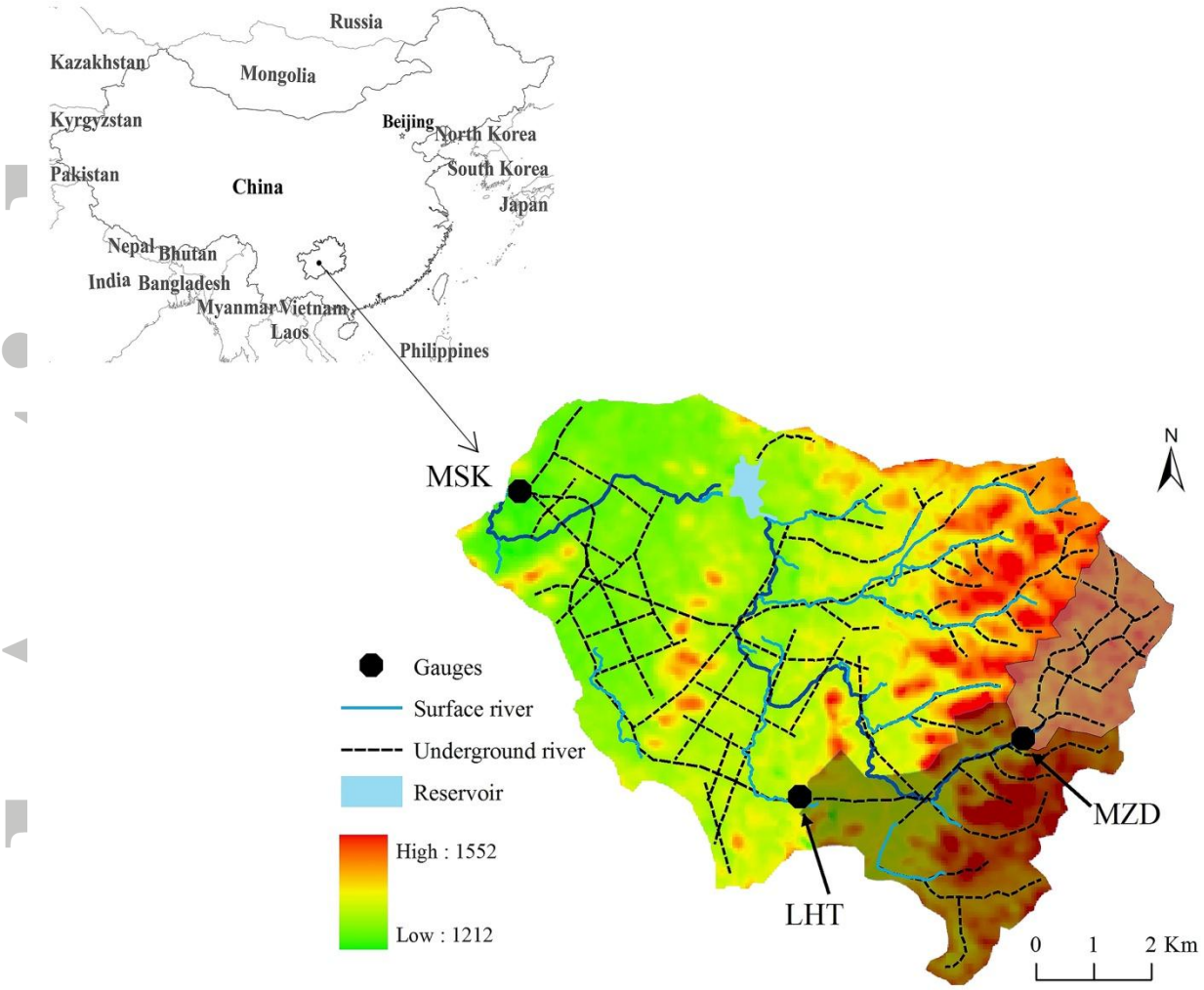

(a)

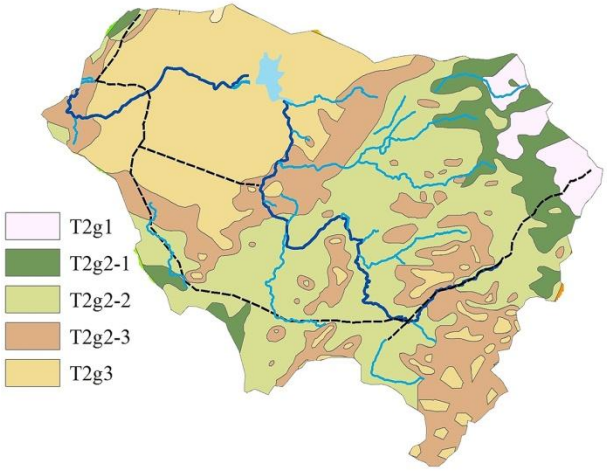

(b)

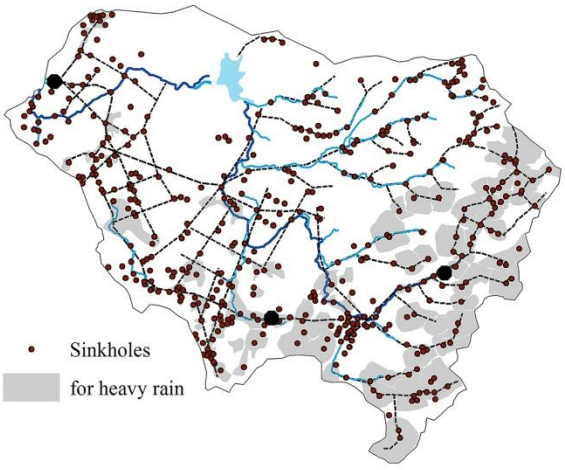

(c)

Figure 1 (a) Topography, surface stream, underground channel network, stations location in Houzhai watershed. (b) Geology (T^2g^1 is interbeded shale and marlstone, T^2g^{2-1} is limestone with vermicular limestone, T^2g^{2-2} is limestone with marlstone, T^2g^{2-3} is limestone and T^2g^3 is dolomite) and (c) Sinkhole location and its drainage area.

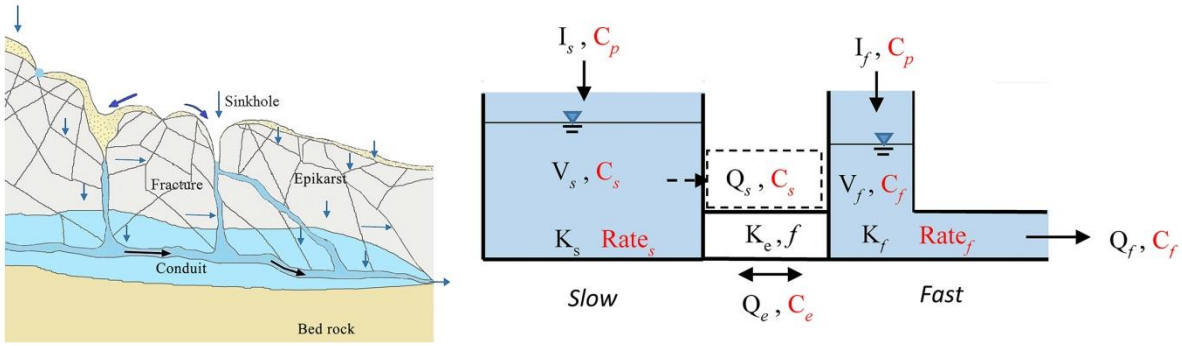

Figure 2 Structure of the coupled flow-tracer model (modified from Rimmer and Hartmann, 2012; Hartmann et al. 2014) represented by fast and slow flow reservoirs (The definitions of symbols are list in Appendix A).

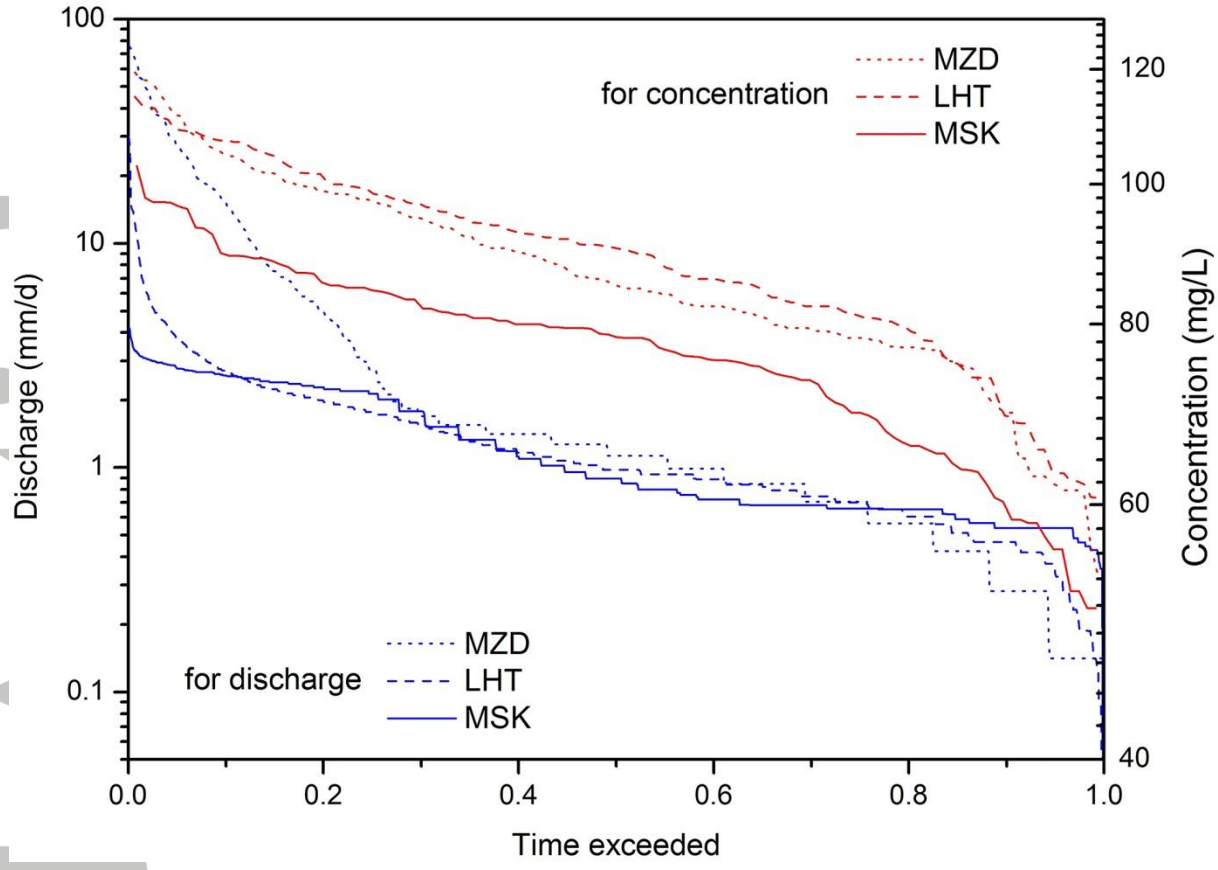

Figure 3 Flow and concentration duration curve at MZD, LHT and MSK (based on 1996 to 2001). The headwater of MZD has the sharpest rise and decline of the hydrograph, while in the middle and downstream, underground flow attenuates and the flow duration curves become relatively smooth. And the variability in the solute concentration is similar at the three sites.

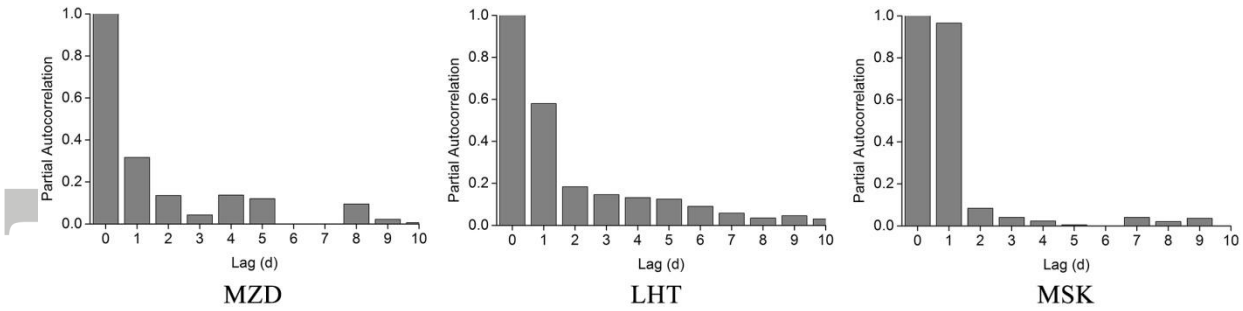

Figure 4 Partial autocorrelation analysis of discharge for the time-lags in three catchments.

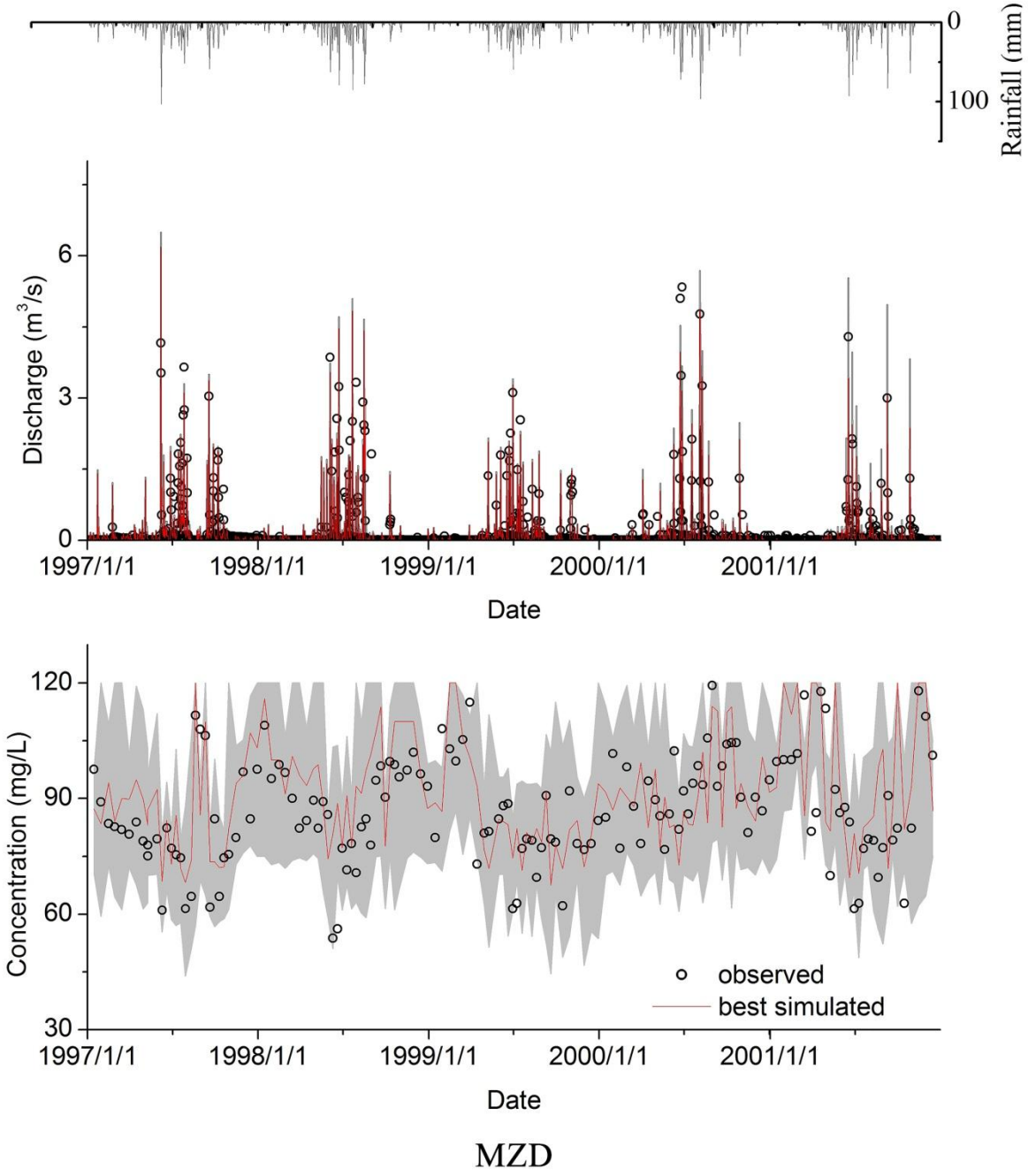

Figure 5a

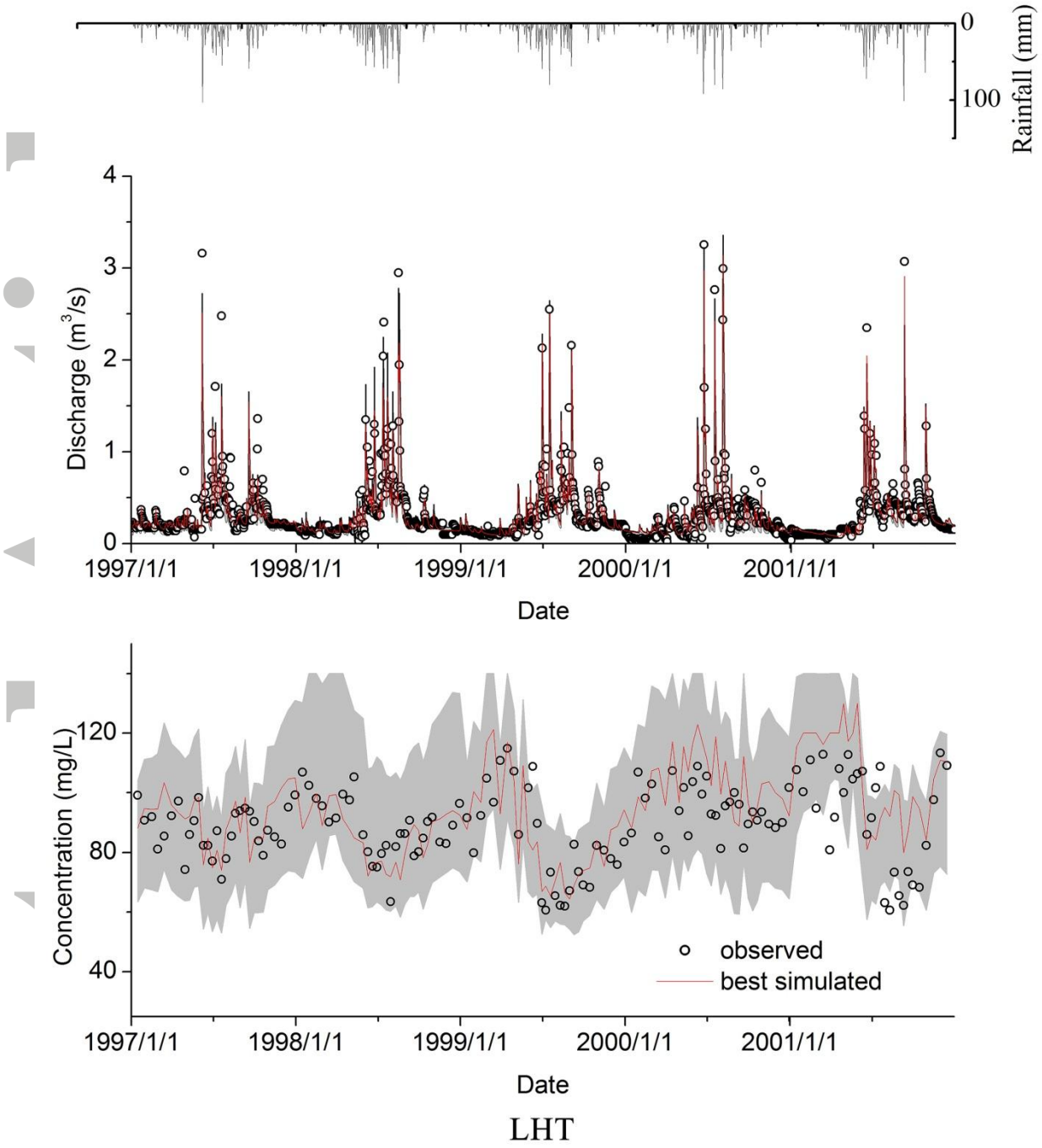

LHT

Figure 5b

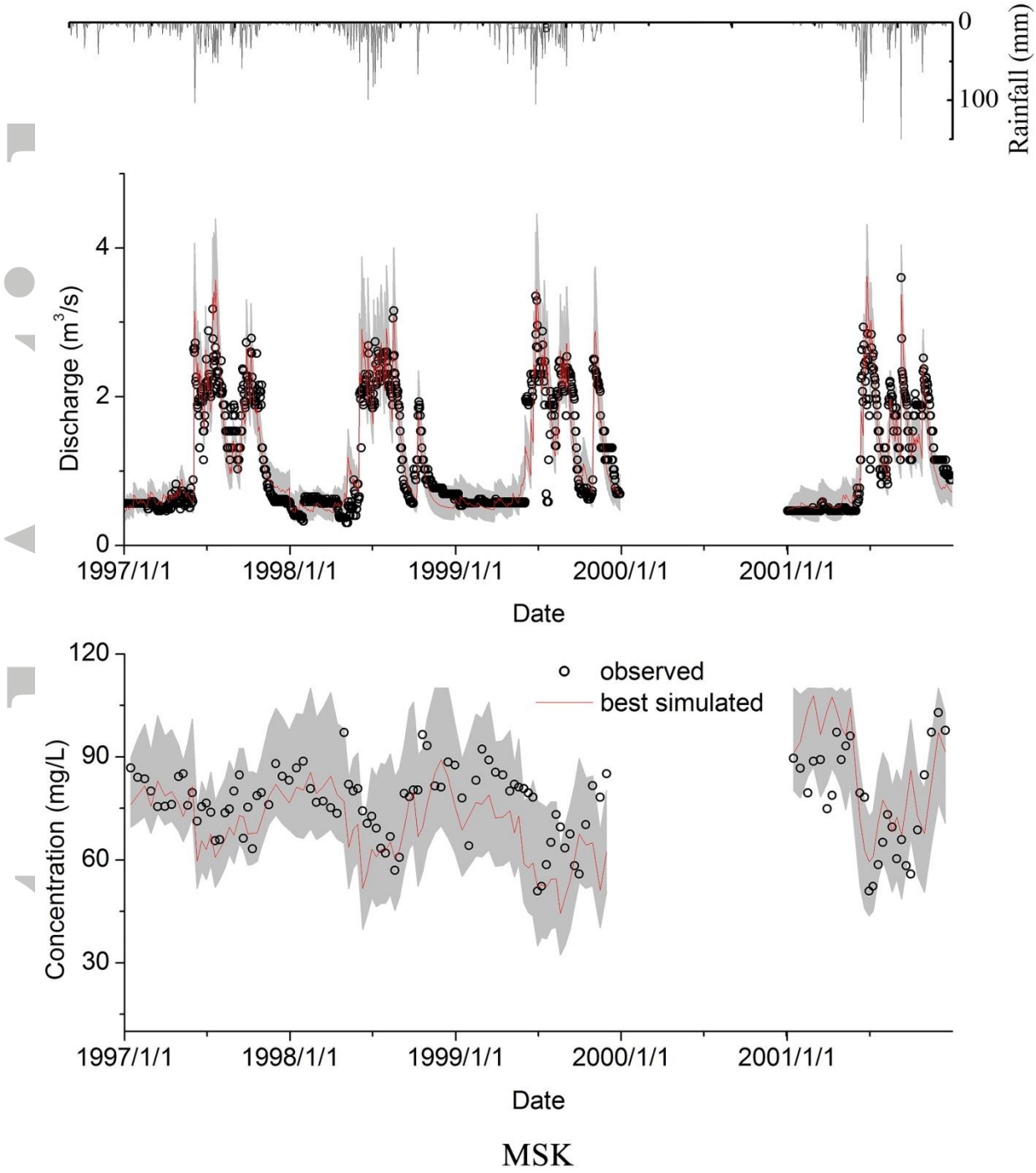

Figure 5c

Figure 5 Observed stream discharge and Mg+Ca concentration during the study period, and discharge and concentration simulations for the best 500 parameter sets.

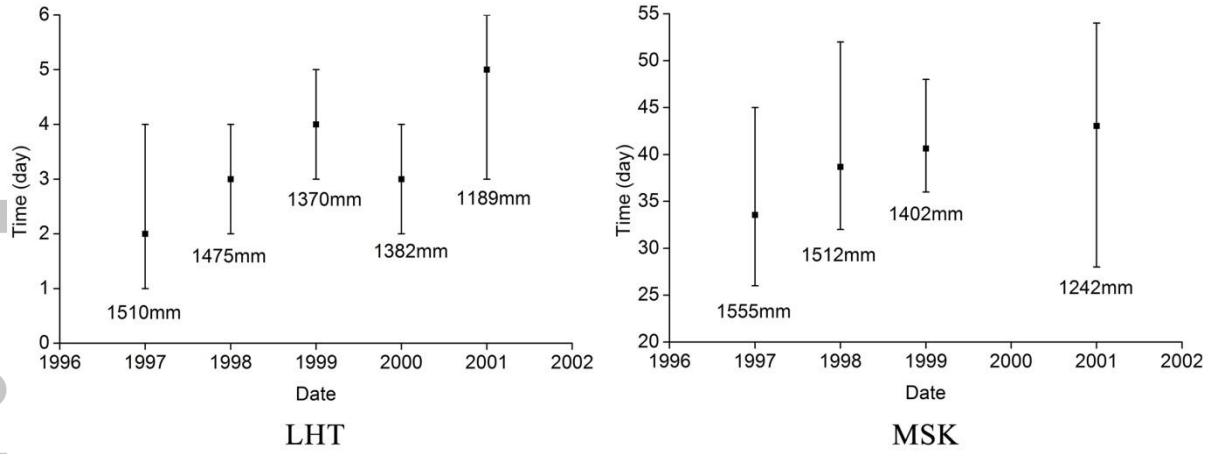

Figure 6 Hydraulic turnover time variation with rainfall amount at LHT and MSK. There is no obvious difference in hydraulic turnover time for MZD in each year because of the short response time of discharge to storage.

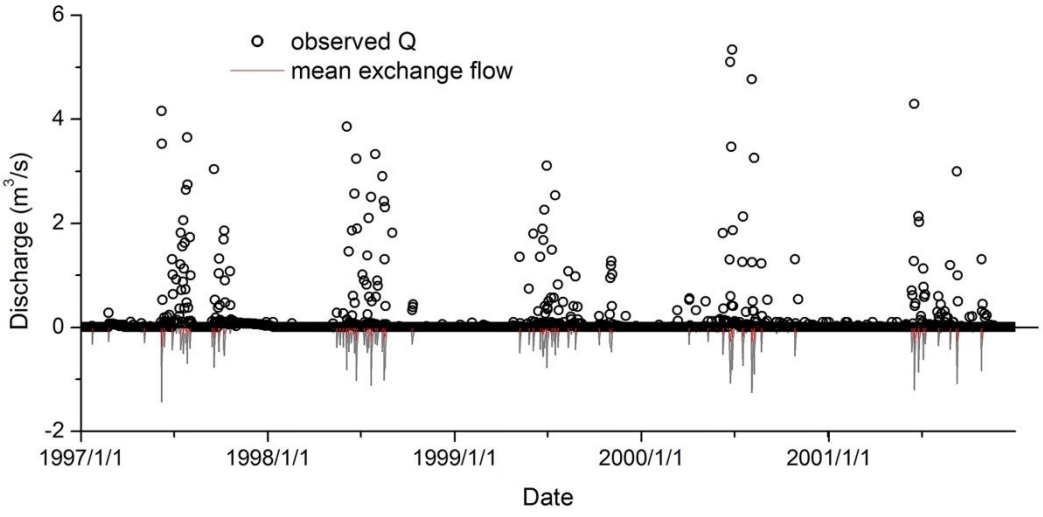

MZD

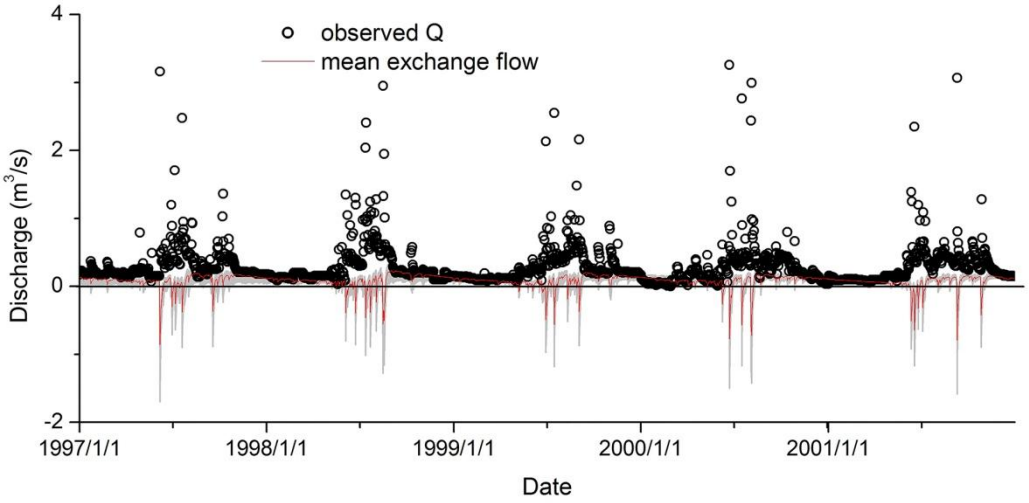

LHT

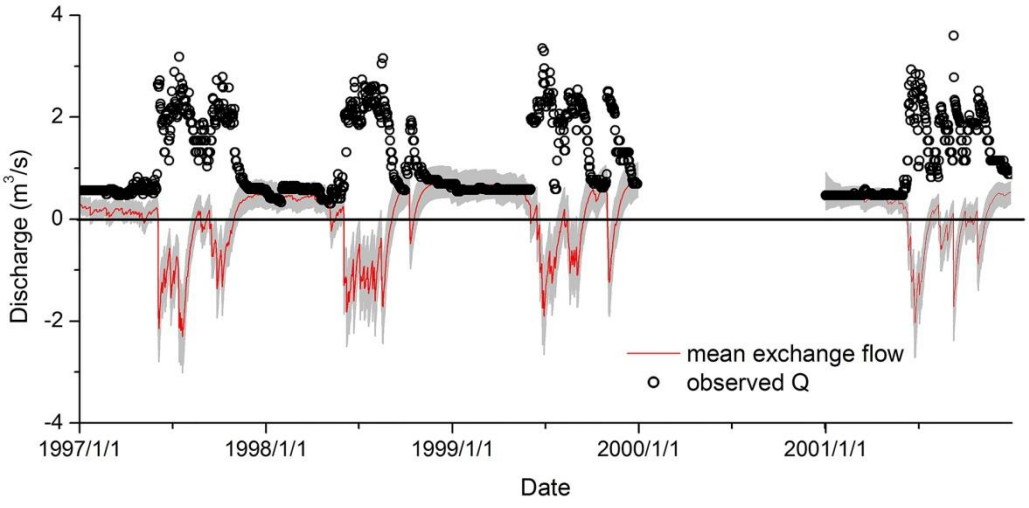

MSK

Figure 7 Flow exchange between fast and slow flow system at the 3 study sites. Positive values show flux from slow to fast flow system and negative values flow from fast to slow flow system.

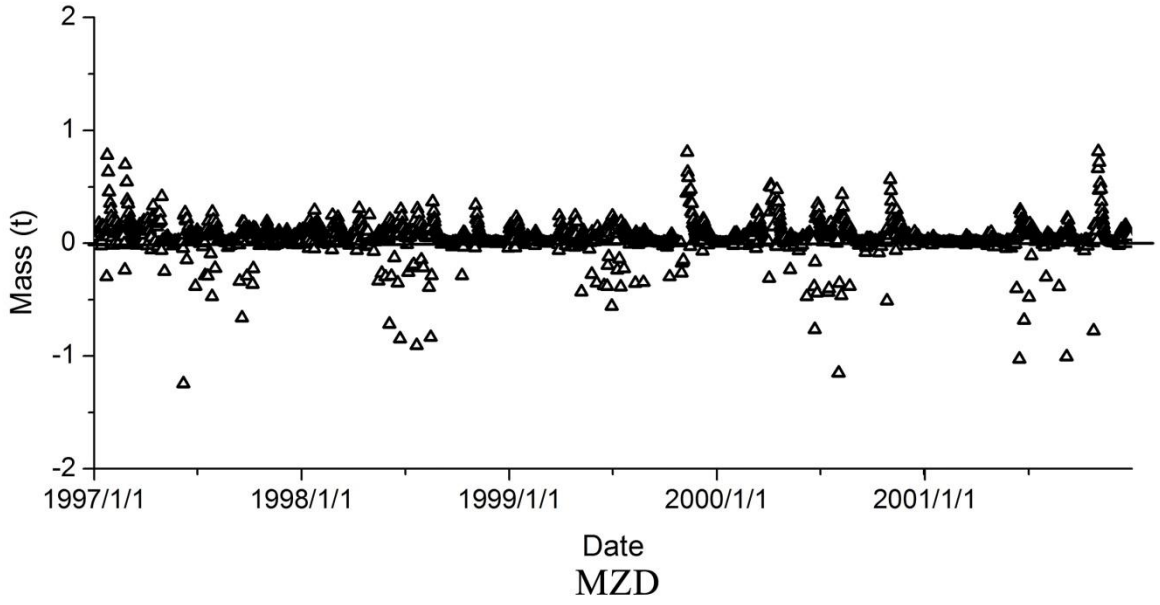

MZD

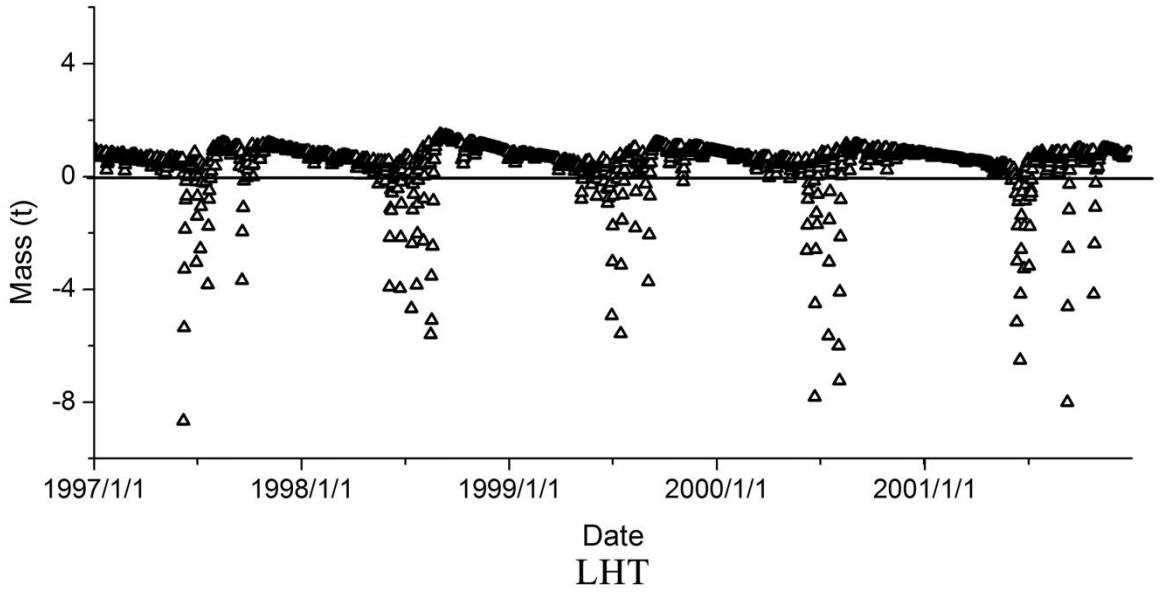

LHT

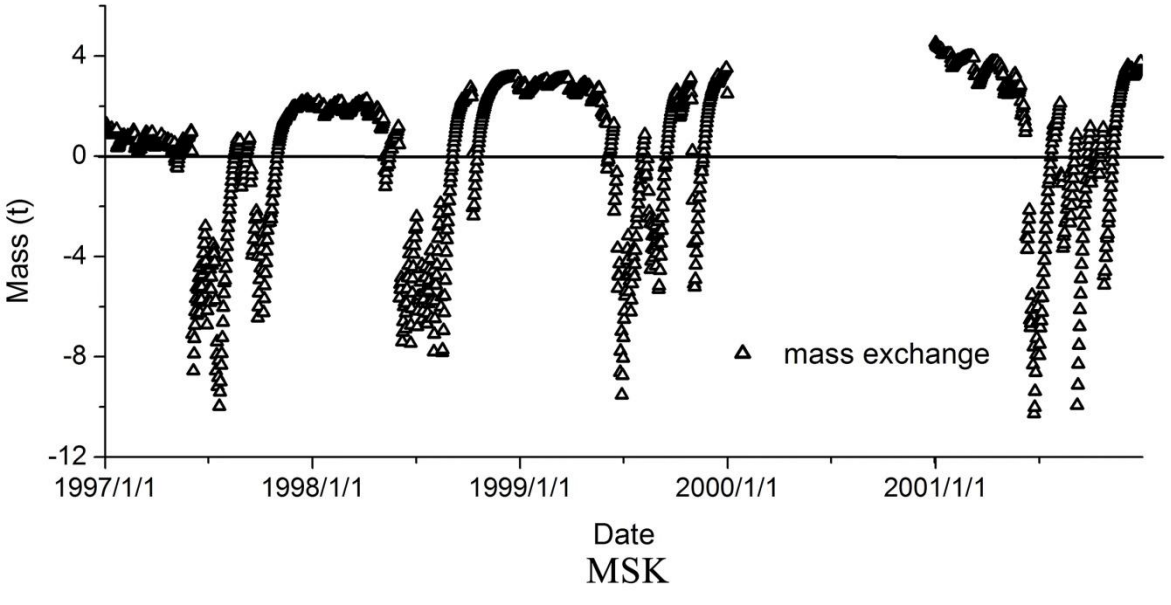

MSK

Figure 8 Mass exchange of Ca+Mg between fast and slow flow system at the 3 study sites. Positive values show mass from slow to fast flow system and negative values mass from fast to slow flow system.

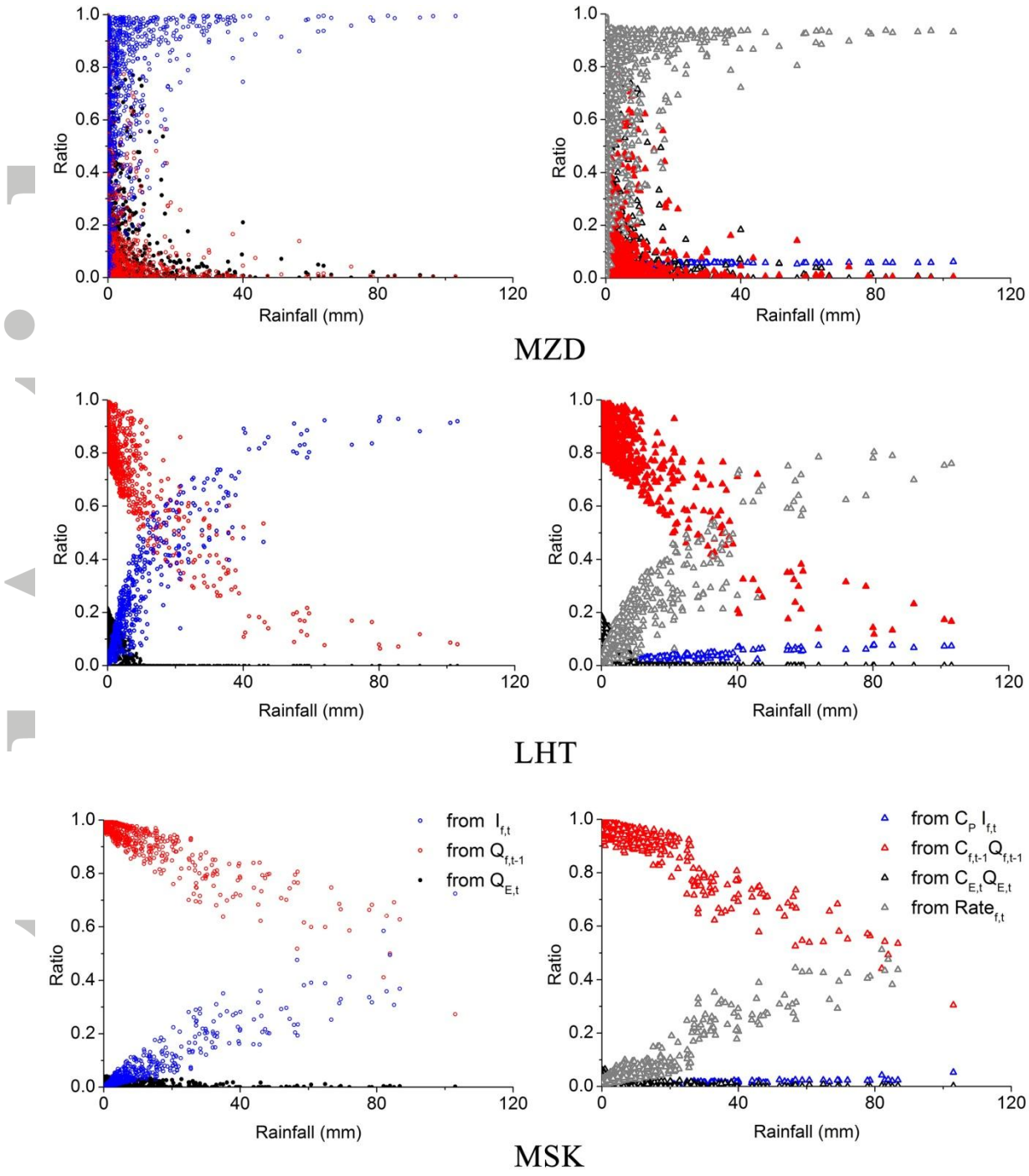

Figure 9 Composition variation of discharge on the left and mass of Ca+Mg on the right for MZD, LHT and MSK.